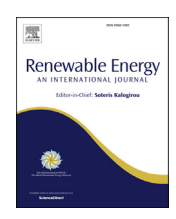


Contents lists available at ScienceDirect

Renewable Energy

journal homepage: www.elsevier.com/locate/renene



Impacts of coexisting buildings and trees on the performance of rooftop wind turbines: An idealized numerical study



Xiantao Fan ^a, Mingwei Ge ^b, Wei Tan ^a, Qi Li ^{c,*}

- ^a School of Chemical Engineering and Technology, Tianjin University, Tianjin, PR China
- ^b School of Renewable Energy, North China Electric Power University, Beijing, PR China
- ^c School of Civil and Environmental Engineering, Cornell University, Ithaca, NY, USA

ARTICLE INFO

Article history:
Received 19 March 2021
Received in revised form
12 May 2021
Accepted 14 May 2021
Available online 29 May 2021

Keywords: Rooftop wind turbines Street trees Large eddy simulation Urban environment

ABSTRACT

In response to the rapid growth of energy consumption in urban cities, rooftop wind turbines (RWT) have emerged as a powerful technique for providing sustainable energy and strategically minimizing the carbon footprint of buildings. However, significant knowledge gaps exist regarding how RWT respond to the complex urban environmental flows modified by the coexisting buildings and trees. This study conducts idealized numerical experiments using an open-source large-eddy simulation model to investigate the interactions between actuator-disc turbines, street trees and buildings. We found that trees taller than the mean building height modifies the existing roof-level strong shear layer by extracting energy from the mean momentum. A significant change in the mean kinetic energy budget is induced, drastically increasing turbulence production of the flow, which leads to lower power output of RWT. Trees lower than the buildings hardly alter the mean flow field but they reduce turbulence production near the roof level. As a result, improved power output (16%) and decreased normalized power fluctuation (5.2%) are observed compared to the control case without trees. The results highlight that it is important to assess effects of different street tree morphologies on the performance of RWT in their design and implementation processes.

© 2021 Elsevier Ltd. All rights reserved.

1. Introduction

Urban environment hosts more than 50% of the world population and the trend of rapid growth in energy consumption (56% from 2010 to 2040) continues in this century [1]. Cities and urban population thus face unprecedented challenges in achieving sustainability, which require innovative strategies for renewable energy to meet the surge in electricity demands.

Recently, there has been an increasing interest in the potential of rooftop wind turbines (RWT) in the built environment for distributed renewal energy generation [2,3]. RWT can be considered as mini- or micro-turbines with small swept areas ≤200 m², low hub height<50m, small rotor diameters<5−10m and rated capacities<50Kw [1,4,5]. Such environmentally friendly and cost-effective modern small rooftop wind turbines are ideal for functioning as an energy source to meet household electricity demands [6,7].

In general, in realistic urban environments, it is likely that both buildings and urban vegetation, especially tall vegetation like street

* Corresponding author. E-mail address: ql56@cornell.edu (Q. Li). trees are present during the operation of RWT. As illustrated in the schematic in Fig. 1, when an internal boundary layer develops over an array of buildings with RWT, the interactions between buildings, street trees and turbines are expected to jointly impact the flow (See Fig. 1). Buildings increase turbulence intensity and mean velocity through acceleration effect of the roof shapes, which is supposed to enhance the power of RWT [8]. Trees, however, extract mean momentum from the flow and thus are expected to reduce the mean power output of RWT. To date, researchers almost exclusively focused on how flows over complex urban buildings impact the performance and efficiency of RWT without the presence of urban vegetation, in terms of both the flow details and wake developments. For instance, Tabrizi et al. [9] and Abohela et al. [10] conducted computational fluid dynamics simulation in the built environment showing that the turbine abilities are particularly sensitive to the building height and shape, roof shape, wind direction and turbine hub height. Peng et al. [11] investigated the wind flow characteristics and wind energy potential over the flat rooftops of tall buildings through wind tunnel testing, showing that wind energy on the roof is more sensitive to the building width ratio, and it can be amplified by 1.6–2.7 compared to case without buildings. Balduzzi et al. [12] found a positive influence on the

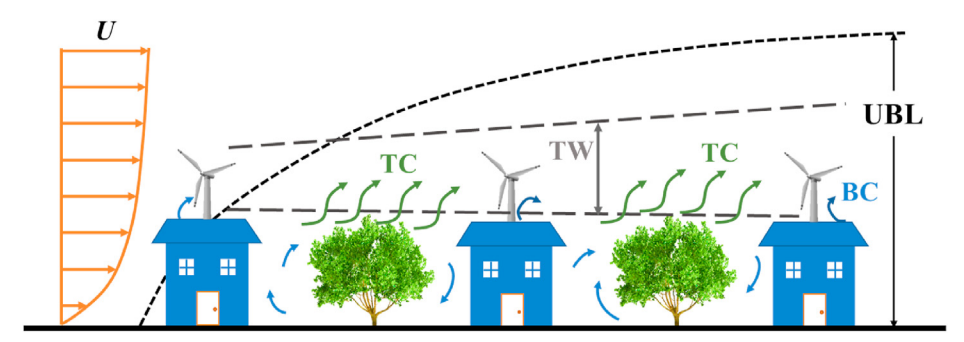


Fig. 1. Schematic diagram of the flow transport in the urban area with rooftop wind turbines, where the gray dashed line represents to turbine wakes (TW) of rooftop wind turbines; green arrows represent the interactions between tree canopy (TC) and TW; and blue arrows indicate influence of the building canopy (BC).

velocity increment in the rooftop area with an optimal sloping angle of 8°, that will ensure a further increase (up to 12%) of the wind energy harvesting. Collectively, urban buildings of certain shapes and arrangements can substantially improve the output power of RWT. However, due to high turbulence intensity and complex flows in the urban environment, fluctuations in the mean power of rooftop turbines could be a bottleneck for efficient operations. This issue has received relatively little attention previously and will be one of the focuses in this work.

In addition, as shown in Fig. 1, the aerodynamics of the tree canopy (TC) and building canopy (BC) are critical for the evolution of rooftop turbines wakes [13–15]. The preliminary wake recovery was related to turbulence [16–18], with the finding of significant positive correlation between the turbulence intensity and wake recovery. Then, the interaction between the wind-turbine wake and a downstream building array was undertaken by Ge et al. using large-eddy simulations (LES) [19]. It is found that a high-pressure region is formed upstream due to the blocking effect of the downstream urban district, which dramatically changes the trajectory of the wind-turbine wake and results in a fast wake recovery, and the wind-turbine wake suppresses the vertical momentum flux and thereby reduces the wind speed in the streamwise streets. Yang et al. [20] evaluated the effects of a threedimensional hill on the wake characteristics of a wind turbine, which found that the hill higher than the turbine hub can promote the recovery of downwind turbine wakes because of the increased entrainment of ambient flow into the turbine wake. The hill enhanced turbulent transport in both spanwise and vertical directions. Similarly, faster recovery of the turbine wake is observed when it was immersed in the wake of buildings, which was caused by the enhanced turbulent transport and convection associated with the secondary mean flow structure behind the cube [21]. Together these studies provide important insights that turbine wakes (TW) can be sensitive to the presence of any urban roughness elements. Nevertheless, there is a lack of understanding on the joint impacts of buildings and tall vegetation (i.e., street trees) on turbine wakes, which may hinder our ability to fully assess the operation of RTW in realistic urban environment.

On the other hand, an extensive body of literature exists on flows over roughness elements, which can consist of tall vegetation (i.e., forest canopy), sharp-edged building obstacles (i.e., building canopy) or coexisting trees and buildings. The canopy aerodynamic drag and complex recirculation and wake patterns lead to the characteristic canopy flows [22]. For example, previous studies have applied LES and wind tunnel experiments over pure vegetation canopies that provides insight of the flow details, turbulent coherent structures and scalar dispersion [23–25]. The impacts of street trees with different morphologies and relative locations on flows over urban building structures have also been investigated [23,24,26–28]. Trees taller than the mean building height were

found to strongly modify the flow and temperature fields [26]. The effects of urban trees are twofold within the urban canopy: on the one hand, they act as a direct momentum sink for the mean flow; on the other hand, they lower the downward turbulent transport of high-momentum fluid, significantly reducing the mean kinetic energy at the heights where people live and buildings consume energy, as concluded in Giometto et al. [23].

Therefore, from these existing evidences of the impact of urban trees on turbulent flows, we postulate that details of the locations and morphologies of the trees with respect to the RWT and buildings critically impact both the mean flow and turbulence. As a result, under certain circumstances, it is likely and will be studied later that their nontrivial interactions can reduce fluctuations in the mean power output of RWT, a desirable outcome in RWT operation. This study is motivated to answer the following research questions: 1) how is the environmental flow altered by the interactions between the wakes of rooftop turbines, buildings and trees? 2) how do different tree morphologies impact the flows and the turbine performance? To investigate the synergistic impacts of RWT and a mixed urban canopy consisting of buildings (i.e. the bluff-body roughness elements) and trees (e.g. the porous roughness elements), we will conduct numerical experiments using large-eddy simulation (LES) modeling.

2. Numerical setup

2.1. Modeling the aerodynamic effects of trees and turbines in LES

2.1.1. Governing equation

LES is a high-fidelity method to simulate the wake of wind turbine farm as well as flows over complex canopy [29,30]. In the current LES model, the buildings/obstacles are resolved using the immersed boundary method [31,32], the RWT are actuator-disc [33,34] and the urban trees are parameterized [26]. The current LES model has been widely applied and validated for flows over complex canopy and wind turbines [32,35]. For neutral condition, the continuous and filtered momentum governing equations are given by

$$\frac{\partial u_i}{\partial t} + u_j \left(\frac{\partial u_i}{\partial x_j} - \frac{\partial u_j}{\partial x_i} \right) = -\frac{1}{\rho_0} \frac{\partial p}{\partial x_i} - \frac{\partial \tau_{ij}}{\partial x_j} + F_i + B_i + T_i + d_i$$
 (1)

$$\frac{\partial u_i}{\partial x_i} = 0 \tag{2}$$

where t denotes time; u_i is the resolved velocity vector and i=1,2,3 corresponds to the streamwise direction x, spanwise direction y and vertical direction z, respectively; ρ_0 is the density of air which is assumed to be constant without loss of generality; p is the modified pressure; τ_{ij} is the deviatoric part of the sub-grid stress tensor; F_i is

the body force driving the flow (here simply a homogeneous steady horizontal pressure gradient along the streamwise direction); B_i is the immersed boundary force representing the action of the obstacles (buildings) on the fluid; T_i is the thrust caused by RWT; and d_i is the drag force exerted by the trees.

For spatial discretization, the pseudo-spectral method is used in the horizontal directions and periodic boundary conditions are adopted in both the streamwise and spanwise directions. A stress-free boundary condition on the top boundary and an equilibrium wall model on the ground and building walls [36] are applied in the current LES. The subgrid scale (SGS) stress tensor is modeled using the Lagrangian scale-dependent dynamic Smagorinsky model [36]. The second-order Adams-Bashforth method is adopted for time advancement.

2.1.2. Wall model

As for the equilibrium wall model on the ground and building walls, the second-order central finite difference method is used in the wall-normal direction. It can be expressed by log law [35]:

$$\frac{u}{u*} = \frac{1}{\kappa} \log \left(\frac{z_n}{z_{0m}} \right) \tag{3}$$

where u is the resolved local wall-parallel velocity near the wall; u_* is the friction velocity calculated as the square root of the kinematic wall shear stress; $z_n = dz/2$ is the distance away from the wall in the wall-normal direction; $z_{0m} = 10^{-4}H$ (H is the height of the cubic buildings) is the roughness lengths for momentum [37,38]. The instantaneous wall stress can be correlated with the filtered velocity $u_i(i=1,2)$ of the first grid node above the surface through:

$$\tau_{w}(x,y) = -\left[\frac{\kappa}{\log((dz/2)/z_{0m})}\right]^{2} \sqrt{u_{1}^{2}(x,y,dz/2) + u_{2}^{2}(x,y,dz/2)} \cdot u_{i}$$
(4)

2.1.3. Thrust force of wind turbine and drag force of tree canopy

The RWT is simplified as an actuator disc (ADM), which has been verified with different turbine models (including ADM-R and ALM) and experimental results to show the accuracy and consistence of large eddy simulation (LES) with ADM [19,39]. The results based on ADM neglect the rotation effect resulting in underestimating the turbulent wake in the near-tip area. However, it is still an effective approach to simulate the wake of RWT. The thrust force T_i is calculated by:

$$T_{i} = -\frac{1}{2}\rho C_{T} \frac{{U_{d}}^{2}}{(1-\alpha)^{2}} \frac{\pi}{4} D^{2}$$
 (5)

where C_T is the thrust coefficient, U_d is the velocity of actuator disc, $U_d = U_\infty(1-\alpha)$, α is the axial induction factor $\alpha = (1-\sqrt{1-C_T})/2$, D is the diameter of the disc. In the current LES model, the thrust of each turbine can be expressed as:

$$T_{i} = -\frac{1}{2} \frac{\pi}{4} D^{2} \rho C_{T}^{\prime} \langle \overline{u}_{d}^{T} \rangle^{2} \Re(x) \widehat{e}_{1}$$
 (6)

where C_T' is the local thrust coefficient, $C_T' = C_T/(1-\alpha)^2$; herein, a typical operating case of the wind turbines is selected with $C_T = 0.75$, which corresponds to $\alpha = 1/4$ and $C_T' = 4/3$ according to previous works [19,40]; $\langle \overline{u}_d^T \rangle$ is the disc and time-averaged velocity; $\Re(x)$ is the smoothed normalized indicator function to distribute the turbine thrust force; \widehat{e}_1 is the unit vector pointing outward from the disc in the direction of the flow.

The drag force d_i of urban tree is parameterized using the same

approach as in Shaw and Schumann (1992) and Pan et al. (2014).

$$d_i = -C_d P_i a(z) |u| u_i (7)$$

where C_d is the drag coefficient, a(z) is the leaf area density (m^2/m^3) and P_i is the projection coefficients. C_d is 0.40 in all the simulations considered in this study based on laboratory experiment. $a(z)P_i$ gives the effective leaf area density facing the ith direction. P_i is adopted based on well-documented empirical results for vegetation canopy, where $P_x = P_y = 0.28$ and $P_z = 0.44$ [25,26]. The vegetation canopy is assumed to be horizontally homogeneous such that P_i and a(z) are functions of height (z) only. An empirical relation found by Lalic and Mihailovic (2004) [41] in Eq. (8) for the leaf area density a(z) is implemented here. The model is shown to be applicable for vegetation canopy for a wide range of leaf-area-index (2–20).

$$a(z) = a_m \left(\frac{h - z_m}{h - z}\right)^n \exp\left[n\left(1 - \frac{h - z_m}{h - z}\right)\right]$$
 (8)

where n=6 for $0 \le z \le z_m$; n=1/2 for $z_m \le z \le h$. a(z) depends on three parameters, which are the tree height h, maximum value of leaf area density a_m at corresponding height z_m . Note that the parameterized trees are simplified as cuboid in the present work. Thus, the typical geometrical parameters of trees include of height h and the tree crown size R_t . The values of these parameters are shown in Section 2.2.

2.2. Details of the numerical setup

The computational domain, presented in Fig. 2, is an idealized urban area with coexisting buildings, street tress and RTW. Similar to Calaf et al. (2013) [33] that examines the fully developed turbulent flow an 'infinite' wind farm, here we make the same assumption for the urban area and a horizontally periodic boundary condition is imposed. The computational domain has a dimension of $L_x \times L_y \times L_z = 12H \times 6H \times 6H = 240 \text{ m} \times 120 \text{ m} \times 120 \text{m}$, and the sufficiency of vertical length $L_z = 6H$ has been verified compared with $L_z = 8H$ (the results are shown in Fig. A1 of Appendix). Same grid scale dx = dy = dz is set in streamwise, spanwise and vertical directions with resolution $N_x \times N_y \times N_z = 240 \times 120 \times 120$ grid points. Thus, the actuator disc of each wind turbine has a resolution of 5×5 grid points, and each building has $20 \times 20 \times 20$ points. 12 cubic buildings with a height of H are used to represent urban area with the aspect ratio H/ w = 0.5, whose space is twice wider in streamwise than that in spanwise. Note that the trees with various heights are placed between the buildings, and the wind turbine is placed at the center of the rooftop. The buildings are placed symmetrically in the computational domain. The flow is driven by a constant streamwise pressure gradient. The grid resolution is previously studied for the present method in urban environment, which shows that 8 grid points is sufficient to resolve the cube in each direction in order to get gridinsensitive results [42,43]. Further, 16 grid points resolving the cube for urban-tree environment also provide reasonable results [26]. Thus, the current setup of 20 grid points is adequate for the urbantree-turbine simulations. All the cases are run for 50 eddy turnover times (one eddy turnover time, T_{ETO} , is defined as the vertical domain height divided by the friction velocity, i.e. $t/T_{ETO} = tu^*/L_z$, $u^* = 0.45$ m/s). To get the mean quantities of the flow, the time-space averaging is made for the instantaneous flow field. The time window of temporal averaging is set as the last 25 eddy turnover times, where the sufficiency has been confirmed. Thereinafter, the upper symbols < > and - refer to horizontal spatial average and time average, respectively.

As shown in Table 1, 13 cases of simulations were conducted to

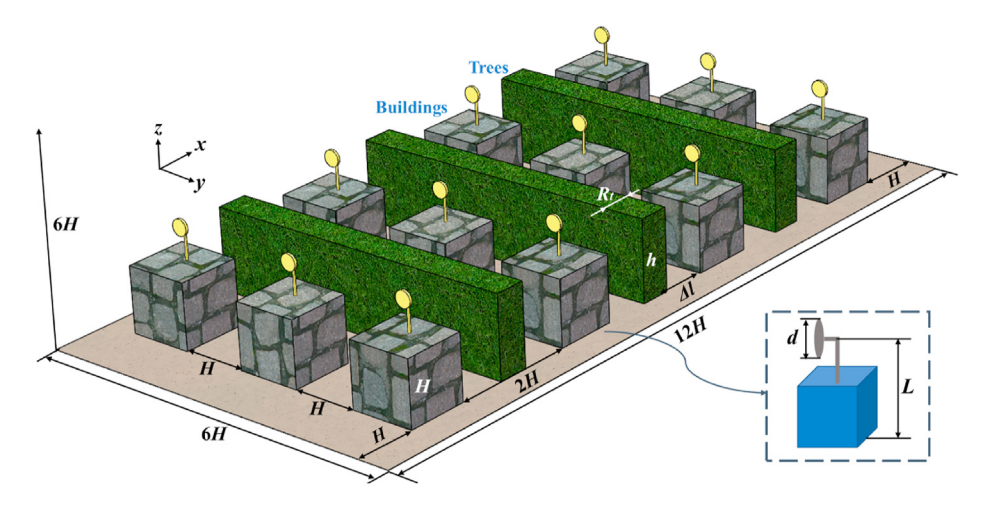


Fig. 2. Scheme of the three-dimensional computational domain with buildings (represented by cubes), rooftop wind turbines (based on actuator-disc model) and parameterized trees (modeled by cuboids with the tree crown of size, R_t).

study how urban buildings and street trees of different morphologies impact the wake of RWT. The symbols "W" and "T" represent wind turbines and urban trees, respectively. W1T1, W1T2 and W1T3 were responsible for interpreting the impact of varied tree heights; W1T2-F and W1T2-B were set for investigating the effect of tree location; W1T4 is applied to analyzing the effect of tree canopy size; W2T2 and W3T2 were used to evaluate the influence of building and tree canopies on different height of turbines. W1, W2 and W3 are the corresponding control groups with buildings and turbines but without trees. W0 is the control case with only buildings and OT is the control case with only turbines to obtain the standard wake propagation in wind farms. Fig. 3 illustrates the distributions of the leaf area density of trees for the cases in Table 1.

3. Results and discussions

3.1. Flow field over buildings

We first analyzed the flow field over buildings only in case W0. The normalized time averaged velocity and turbulence intensity in streamwise direction of this area are shown in Fig. 4. Fig. 4a clearly indicates the difference between $\langle \overline{u} \rangle$ above the rooftops and that in the street canyons, especially for $z/H \leq 2.5$. Recirculation between the buildings is observed in the lower part of the street canyon. Strong vertical gradients of $\langle \overline{u} \rangle$ near z/H=1 above the roofs indicate the presence of strong shear layer. Large values of $I_u=0.255-0.213$ (I_u is the turbulence intensity) at z/H=1.5-2 above the rooftop

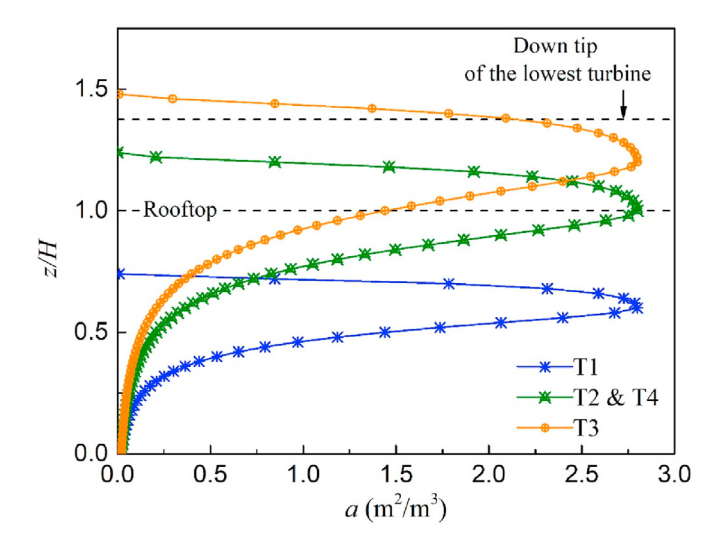


Fig. 3. Vertical distribution of leaf area density a for different tree canopies, where a(z) in T2 and T4 are identical except for different tree crown sizes.

indicate strong flow fluctuations, which is much higher than that in the case without buildings [19]. This means that potentially RWT can be impacted by the shear layer and high I_u due to the buildings. Moreover, the streamwise velocity contour in the horizontal xy-plane (Fig. 4 (c)) at z/H = 0.5 shows that low values of \overline{u} are present in areas sheltered by the buildings in their leeward [42,43]. Next,

Table 1Parameters for different computational cases.

Cases		Rooftop turbines		Trees				
		d/H	L/H	Rt/H	h/H	z _m /h	a_m	$\Delta l/h$
Only turbine	OT	0.25	1.5	-	-	-	_	_
No Tree	W0	_	_	_	_	_	_	_
	W1	0.25	1.5	_	_	_	_	_
	W2	0.25	1.75	_	_	_	_	_
	W3	0.25	2	_	_	_	_	_
With Tree	W1T1	0.25	1.5	0.25	0.75	0.8	2.8	1
	W1T2	0.25	1.5	0.25	1.25	0.8	2.8	
	W1T3	0.25	1.5	0.25	1.5	0.8	2.8	
	W1T4	0.25	1.5	0.5	1.25	0.8	2.8	
	W2T2	0.25	1.75	0.25	1.25	0.8	2.8	
	W3T2	0.25	2	0.25	1.25	0.8	2.8	
	W1T2-F	0.25	1.5	0.25	1.25	0.8	2.8	1.5
	W1T2-B	0.25	1.5	0.25	1.25	0.8	2.8	0.5

the joint impact of the buildings and trees on the turbine wake will be discussed and evaluated.

3.2. Joint impact of buildings, trees and turbines on the flow field

This section first examines the joint impact of tree canopies and turbines with various morphologies on the overall flow filed in urban environment is discussed for answering the first question proposed in Introduction. Fig. 5 shows the normalized time-space average shear strength $d\langle \overline{u} \rangle / dz / \langle \overline{u}(z = H) \rangle H$, in which three typical enhanced shear strength regions can be clearly observed. The first shear strength peak is in the rooftop illustrating that there exists a strong shear layer generated by the buildings. It is remarkable that the trees taller than buildings can modify the strong urban shear layer, corresponding to the second peak at z/H = 1.25 for the cases of W1T2, W1T2-F, W1T2-B and W1T4 (shown in Fig. 5 (a)). The third transitional shear strength region is at the location of turbines. However, such vital transition of shear strength totally coincides with the trees taller than the down tip of turbines as shown in W1T3. In addition, as show in W1T1, the trees lower than the buildings can slightly reduce the shear strength in street canyon but has less impact above the rooftop. Overall, Fig. 5 indicates that the tall tree canopy increases the shear strength, demonstrating that the mean flow is the most sensitive to tree canopy height rather than the location or crown size. Similar conclusions are also obtained in Fig. 5 (b). As reported in Li et al. [26] and Krayenhoff et al. [27], the modification of the tall tree is creating additional shear layer to interact with the existed building shear layer, which is more obvious in the tree with dense foliage and the crown that partially or fully cover the rooftop.

Next the magnitude of the difference between a variable in cases with and without tress ($\langle X \rangle_{VAR}$) is defined in Eq. (9):

$$\langle X \rangle_{\text{VAR}} = \langle |X_{\text{case}} - X_0| \rangle \tag{9}$$

where X_0 denotes the corresponding cases without trees (W1, W2 and W3) and <> indicates averaging over the volume $L_x \times L_y \times L_z$ excluding the solid volume occupied by the buildings. The normalized velocity and Reynolds stress (resolved and subgridscale parts) for all the cases are shown in Fig. 6. The tall trees significantly affect the vertical distributions of velocity and Reynolds stress, especially near the rooftop and within the street canyon with $\langle X \rangle_{VAR} \geq 0.4$. The larger variability in $\langle \overline{u} \rangle_{VAR} / \langle u_{(z=H)} \rangle$ indicates that different tree canopy morphologies and locations result in distinct surface drag. The time-averaged I_u (hereinafter, $I_u = \sigma_u / u_{(z=hub)}$) for cases with tree canopy of different heights are compared with case without the trees, as highlighted in Fig. 6 (c) showing three typical cases W1, W1T1 and W1T2 (the others are shown in Fig. A2 the Appendix). Surprisingly, compared with W1, high values of I_u behind the upstream turbine from z/H = 1 to height of the turbine are lower in W1T1 due to the presence of tree canopy at z/H = 0.75. In contrast, the tall tree canopy W1T2 significantly increase I_{ν} . This may be caused by tall tree canopy exerting a high pressure drag to the flow, leading to an increased transfer of turbulent kinetic energy from the mean flow to turbulence [44]. It will drastically influence the output power of the RWT, and detailed analysis is given in Section 3.5. To summarize, we confirmed that the mean streamwise velocity, Reynolds stress and turbulence intensity are not as sensitive to the location and crown size compared to the tree canopy height.

Next, the spatial distributions of the time-averaged velocity and Reynolds stress in the urban environment are plotted for interpreting the joint impact of buildings, trees and turbines. A unit, consisting of two adjacent buildings and the intermediate street canyon,

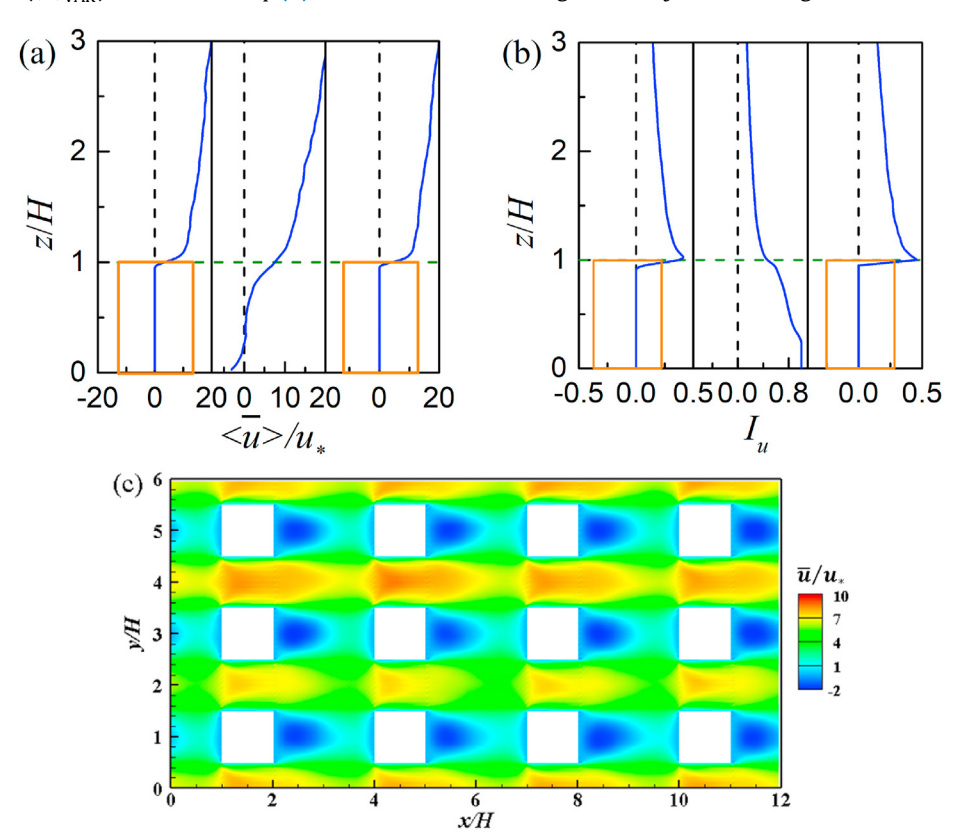


Fig. 4. The vertical profiles of the rooftop and street canyon (a) mean velocity and (b) turbulence intensity. (c) the horizontal xy-plane contour of \overline{u} at z/H = 0.5 in W0 along the streamwise direction, where the flow is from left to right.

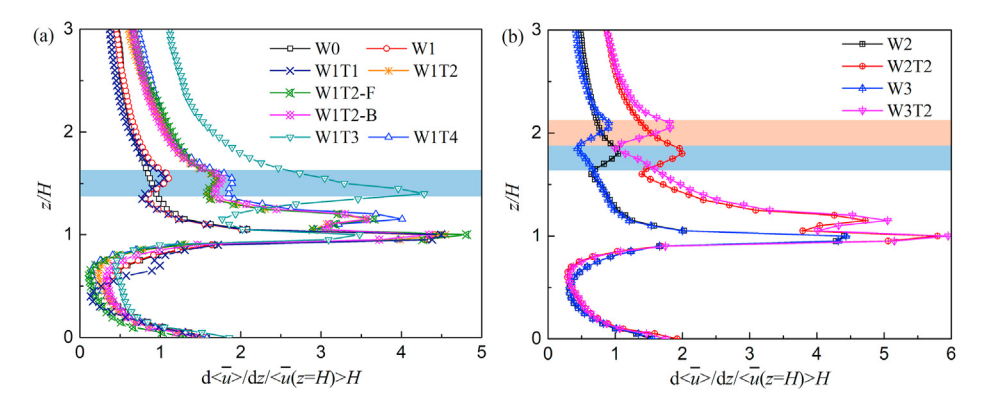


Fig. 5. The normalized time-averaged shear strength for (a) the lowest turbine W1 with different tree canopies, and (b) the two higher turbines, W2 and W3, with the same tree canopy. The block shows the location of turbine disc.

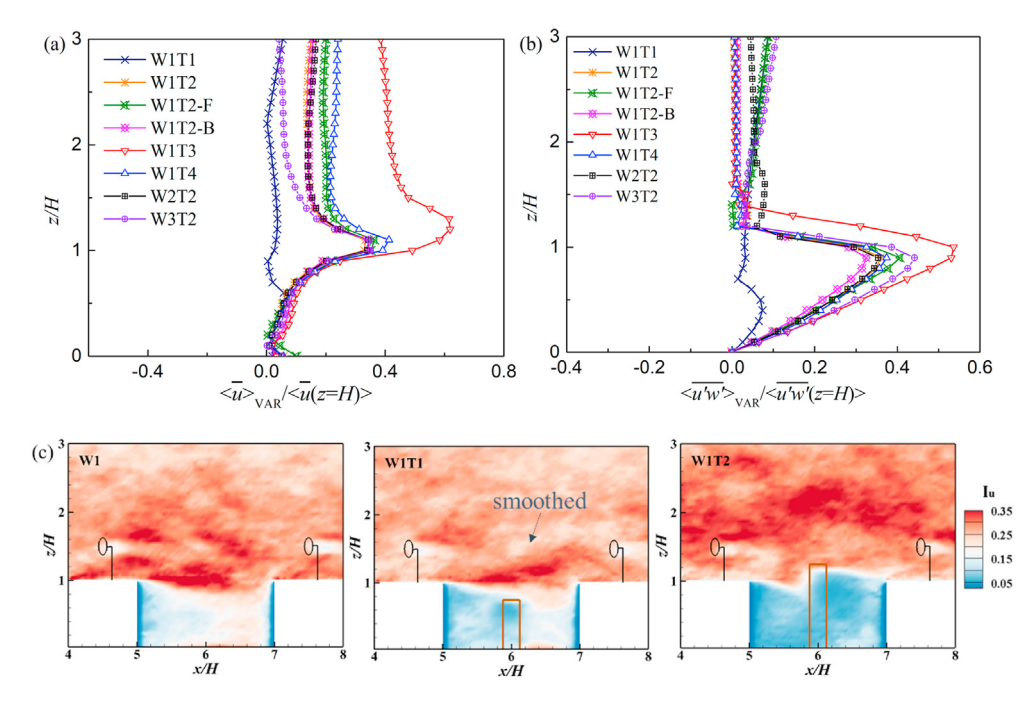


Fig. 6. Comparison between cases of turbines with different tree canopies with their corresponding control cases (a) normalized variance of mean velocity, (b) normalized variance of Reynolds stress, and (c) the time-averaged turbulence intensity for the typical cases W1, W1T1 and W1T2.

in the streamwise direction of the computational domain is selected for presentation, and the normalized velocity contours and streamlines are presented in Fig. 7, where the white block represent the buildings. The spatial patterns of the flow field have been drastically altered due to the presence of the trees, despite seemingly small differences in the horizontally normalized quantities shown in Fig. 6. For the moderate canyon aspect ratio (i.e., building height divided by street width) of 0.5, a clockwise recirculation within the street canyon is formed close to the windward (W0), which is quite characteristic for street canyons with similar aspect ratio [45]. The rooftop turbine (W1) and low urban tree (W1T1) hardly alter the flow recirculation pattern within the street canyon. However, as W1T2, W1T3 and W1T4 shown in Fig. 7, the tall tree canopy alters the location of the recirculation, which is 'locked' between the leeward of the building and the tree canopy, as indicated by the arrows. When the tall trees are placed forward (W1T2-F) or backward (W1T2-B) with respect to the street canyon center line, the flow recirculation is located near the leeward but its horizontal extent decreases or increases, respectively, shown by the arrows in Fig. 7 (e) and (f). As described in Ref. [46], the flow pattern in the

moderate street canyon is dominated by the upstream wake and is sensitive to the pressure drag imposed by the building geometry. Therefore, the urban tree canopy as porous obstacles exert additional drag force, depending on its height, location, and morphology, which modify the effective street canyon aspect ratio and thus drastically changing the flow recirculation within the street canyon. The wake of the lowest turbine (all cases with W1) is not apparent and partially immersed in the shear layer of the building and tree canopies for all cases. On the contrary, the turbine wakes in cases W2, W3 and W3T2 can be clearly observed, since they are too tall to be interfered by the shear layer of buildings and trees (except for W2T2, which is slightly affected by the tall tree canopy). The following analysis of the spatial distribution of Reynolds stress provides consistent results about the impacts of tree canopy.

Fig. 8 depicts the temporally averaged $\overline{u'w'}/u_*^2$. The standard turbine wake in case OT (Fig. 8 (a)) is approximately horizontal, which is consistent with its distribution in Abkar and Porté-Agel [16]. However, as confirmed by W1, $\overline{u'w'}/u_*^2$ caused by the down tip of turbine is totally combined with that of buildings and thus

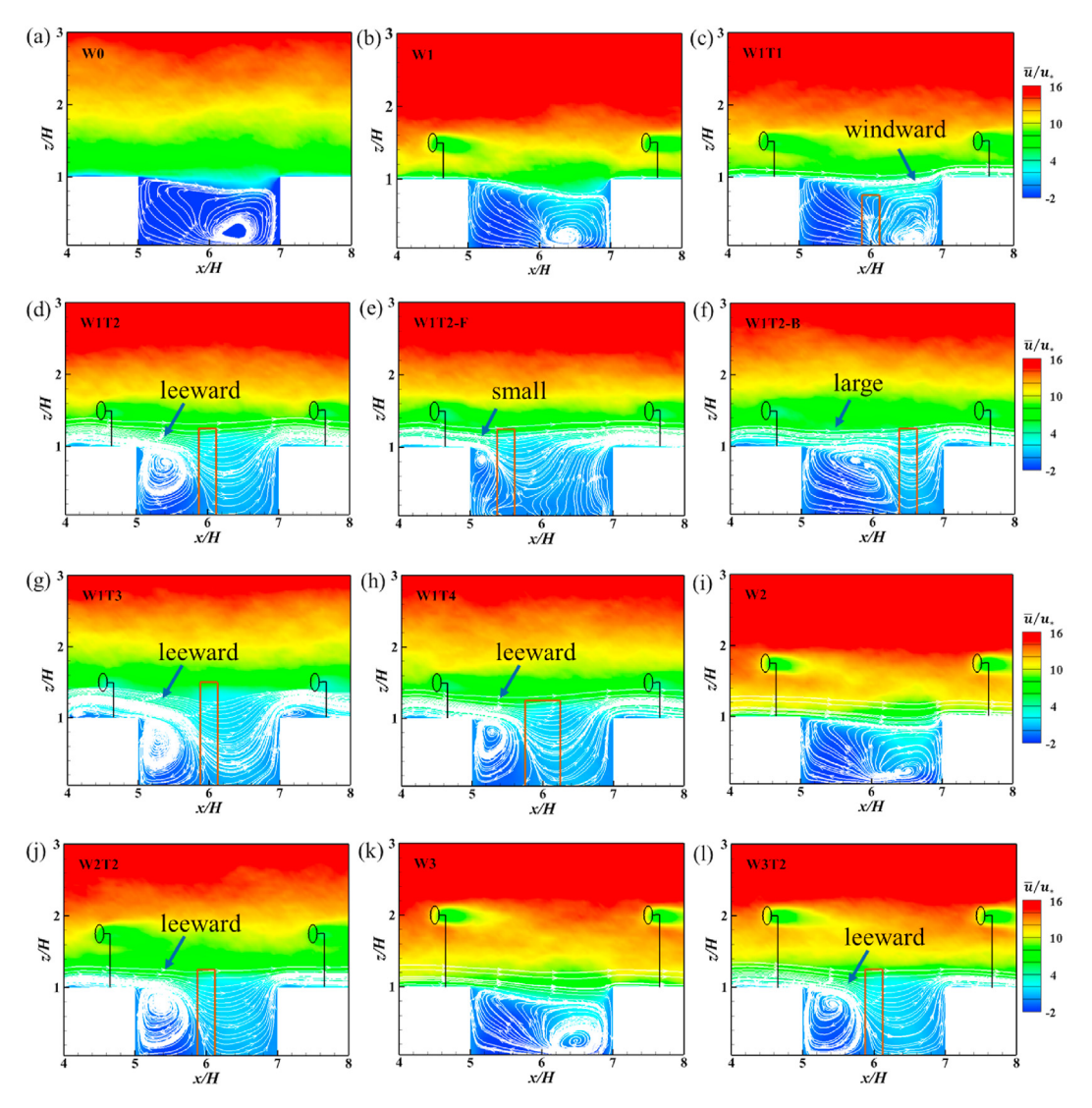


Fig. 7. The normalized time-average velocity contours and streamlines in the middle xz-plane for all the cases listed in Table 1, where the white blocks represent the buildings, the brown block refers to the urban tree and the white lines are the mean streamlines.

the positive momentum flux is suppressed, resulting in a downward shift of negative $\overline{u'w'}/u_*^2$. When the hub height is increased in case W3, the spatial distribution of $\overline{u'w'}/u_*^2$ is almost undisturbed by the urban and tree canopies, similar to those in OT, in which equally positive and negative components are found in the turbine wakes. On the other hand, tall trees (W1T2, W1T3 and W1T4) cause the negative momentum flux of the buildings and turbines combined to preferentially distribute between the building leeward and the tree canopy. For the lower part of the urban street canyon, buildings have the largest contribution to the total drag force, which is in equilibrium with the transport by Reynolds stress [23]. Therefore, the tree canopy lower than Honly slightly increase the magnitude of the Reynolds stress within the street canyon. Conversely, for the urban canopy above the buildings, a significant portion of the vegetation drag force is exerted by the tall tree canopy, resulting in a monotonic decrease of the Reynolds stress [23]. The downward flux of momentum from turbulent motions is suppressed and hindered by the tall tree canopy. Consequently, the urban tree and buildings can affect the wake topology and propagation of the RWT, leading to the change of the performance of the turbines. This aspect will be further analyzed in Sec. 3.5.

3.3. The MKE budget analysis

The mean kinetic energy (MKE) budgets are used to understand which parameters of flow and how buildings, trees and turbines interact with each other in the wake region between two arrays of buildings. The MKE transport equation can be expressed as [16,19,20,47]:

$$0 = -\frac{1}{2} \overline{u}_{j} \frac{\partial \overline{u}_{i} \overline{u}_{i}}{\partial x_{j}} - \frac{\partial \left(\overline{u}_{i} \underline{u}_{i}' \underline{u}_{j}'\right)}{\partial x_{j}} + \overline{u}_{i}' \underline{u}_{j}' \frac{\partial \overline{u}_{i}}{\partial x_{j}} - \frac{1}{\rho} \frac{\partial \overline{p} \overline{u}_{j}}{\partial x_{j}} + \frac{\partial \left(\overline{u}_{i} \overline{\tau}_{ij}\right)}{\partial x_{j}} - \overline{\tau}_{ij} \frac{\partial \overline{u}_{i}}{\partial x_{j}}$$

$$(10)$$

Thus, the spatial-integral MKE budgets in Ω are obtained in Eq. 11- Eq. (16).

$$MC = -\frac{1}{2} \iint_{\Omega} \overline{u}_{j} \frac{\partial \overline{u_{i}u_{i}}}{\partial x_{j}} dydz$$
 (11)

$$TC = -\iint_{\Omega} \frac{\partial \left(\overline{u_i}\overline{u_i'u_j'}\right)}{\partial x_j} dy dz$$
 (12)

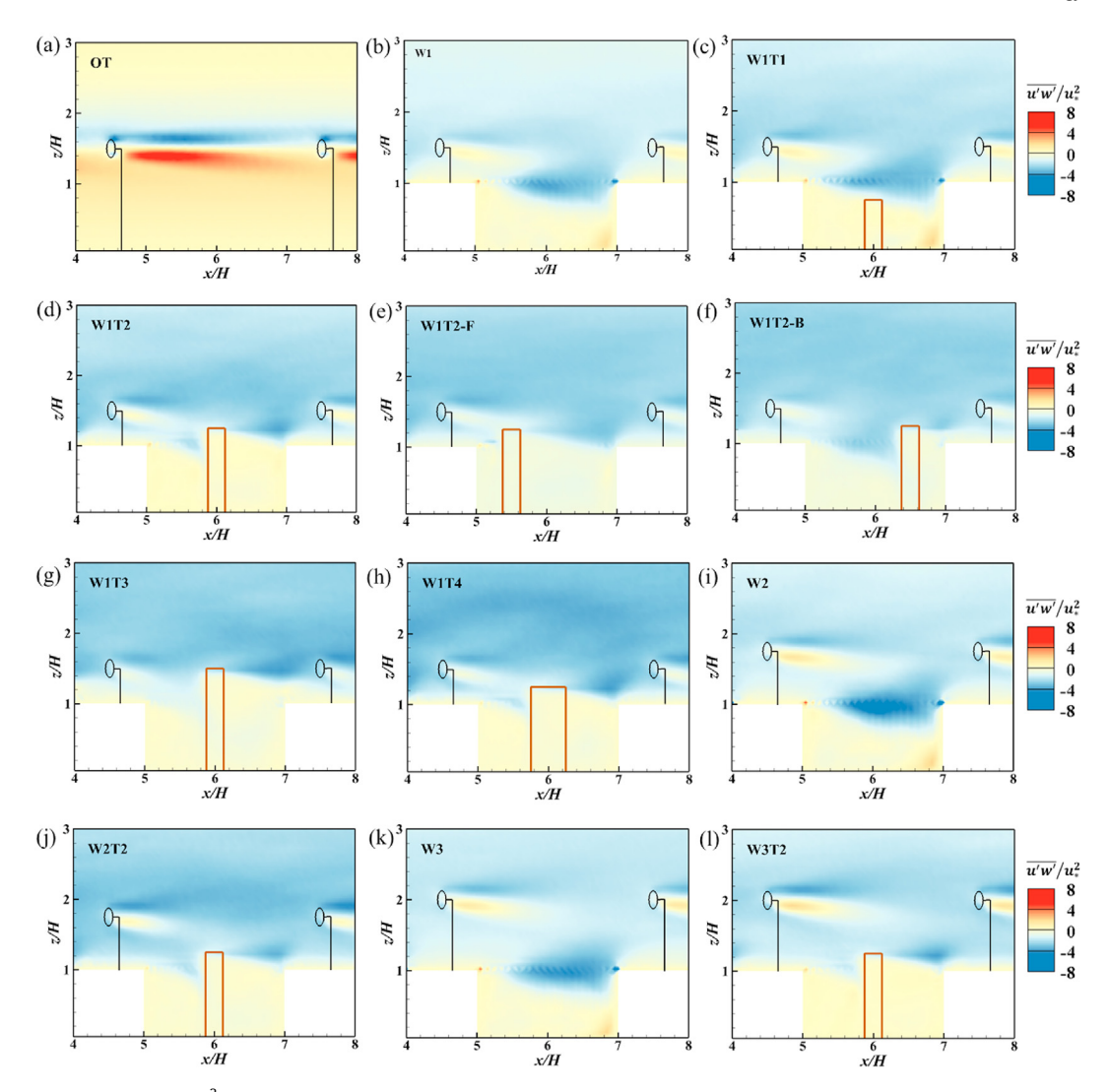


Fig. 8. The normalized time-average $\overline{u'w'}/u_*^2$ in the middle xz-plane for all the case listed in Table 1, where the white blocks represent the buildings and the brown block refers to the urban tree.

$$TP = \iint_{\Omega} \overline{u_i' u_j'} \frac{\partial \overline{u_i}}{\partial x_j} \, dy dz \tag{13}$$

$$PT = -\frac{1}{\rho} \iint_{\Omega} \frac{\partial (\overline{pu_j})}{\partial x_j} dy dz$$
 (14)

$$DF = \iint_{\Omega} \frac{\partial \left(\overline{u_i \tau_{ij}}\right)}{\partial x_i} dy dz \tag{15}$$

$$DP = -\iint_{\Omega} \overline{\tau_{ij}} \frac{\partial \overline{u_i}}{\partial x_j} \, dy dz \tag{16}$$

where MC describes the advection of MKE by mean flow; TC is the turbulent convection, and it describes how MKE is move around by the turbulent eddies; TP is the turbulence production term (loss in MKE, negative production), which represents the energy transported from the mean kinetic energy to the turbulent flow due to the mean shear; PT is the pressure correlation term that describes how MKE is redistributed by pressure gradient; DF denotes the diffusion term, and DP represents the dissipation term. The integral domain Ω for all the cases listed in Table 1 is on the cross sections

with $y \in [y_{hub} - 0.5D, y_{hub} + 0.5D]$ and $z \in [h_{hub} - 0.5D, h_{hub} + 0.5D]$, which is concentrated on the streamwise turbine wake area. All the budgets are normalized by $A\overline{u_{hub}}^3/2D$ with $A = D^2$. The standard MKE budgets of OT in wind farm are presented in Fig. 9 for comparison, where TC and MC are balanced in the far wake region.

As confirmed by the MKE budget in the vertical direction [48], the transport terms of the model canopy (including buildings and trees) indicate that turbulence extracts energy form the free-shear-layer-like flow immediately above the canopy (1 < z/H < 1.5) and redistribute the energy into the other heights. Here, we focus on the MKE budget of the lowest rooftop turbine W1 $(H_{\text{hub}} = 1.5H)$ with different tree canopy morphologies, since it provides crucial information about energy transfer modified by the joint effects of the buildings, trees and turbines.

Fig. 10 shows the MKE budget in the wake region for three representative cases, namely, W1, W1T1 and W1T2. The rooftop and street canyon are regarded as near and far wake region, respectively. The tall tree canopy, such as W1T2, behaves as a porous wall and momentum sink against the horizontal mean flow to decrease \overline{u} , and slightly enhancing the vertical velocity \overline{w} (as the streamlines shown in Fig. 7) in the far wake region. It corresponds to the decrease of MC in W1T2 (Fig. 10 (a)). In addition, the decreased TC (Fig. 10 (b)) and TP (Fig. 10 (c)) terms in W1T2 indicate

that the mean energy is dominantly moved around by the turbulent eddies and transformed to turbulent kinetic energy (TKE) with loss of MKE when going through the tall trees. The loss of MKE is also partially caused by the additional strong shear force (see the second peak in Fig. 5). The higher TKE can lead to the high turbulence intensity in W1T2 (see Fig. 6 (c)). On the other hand, according to Eq. (12) and Eq. (13), the change of TC and TP reflects the decrease of $\overline{u'w'}$, which is also confirmed by the contours in Fig. 8, where $\overline{u'w'}$ of high magnitude (i.e., more negative) is restricted upwind of the tall trees before decreasing downwind. The dissipation of MKE in W1T2 is enhanced in the far wake region, resulting from the drag by the tree foliage as confirmed by the increased *DP* (Fig. 10 (f)) [27]. Note that the higher *DP* is mainly controlled by the SGS dissipation term instead of the dissipation directly from the mean flow [48]. Correspondingly, the viscous diffusion DF is decreased due to the same drag force of tree foliage (see Fig. 10 (e)). Furthermore, due to the strong pressure gradients present in the urban environment. the non-negligible pressure transport PT dominates within the wakes [19,49]. With respect to canopy and near-canopy levels, PT of tree operates in a similar function to turbulent diffusion, extracting energy form the near canopy top, and acting as an energy supply for the other regions [50]. The obstacles, such as buildings and trees (especially for dense foliage $a_m = 2.8$) induce significant pressure gradients in the horizontal direction. The pressure transport term PT dominates in the MKE budget compared to other terms (see Fig. 10 (d)), especially for the tall tree case W1T2. It can be inferred that higher level of PT in case W1T2 compared to the other two cases at $x/H \sim 6$ acts to promote the recovery of wake in the far wake region.

The current integral domain Ω is too high to study the influence of the low tree canopy case W1T1. Therefore, the MKE budgets of W1T1 closely resemble that of W1 in Fig. 10. The low tree canopy has little effect on the alteration of urban flow fields as presented in Figs. 7 and 8, however, the turbulence intensity near the urban canopy top is indeed modified (see Fig. 6 (c)). Fig. 11 depicts the contours of turbulence productions TP to highlight the modification by the low tree canopy within the street canyon. The high magnitude of TP near the shear layer produced by the buildings (Fig. 11 (a)) is significantly reduced by the low tree canopy W1T1 (Fig. 11 (b)) due to its reduction of the shear strength for z/H < 1 (see Fig. 5 (a)). It also indicates that less MKE is transformed to TKE, resulting in smaller turbulence intensity in Fig. 6 (c) than that in W1.

The contributions of buildings and trees to the MKE budget also differ, which subsequently affect the wake development and

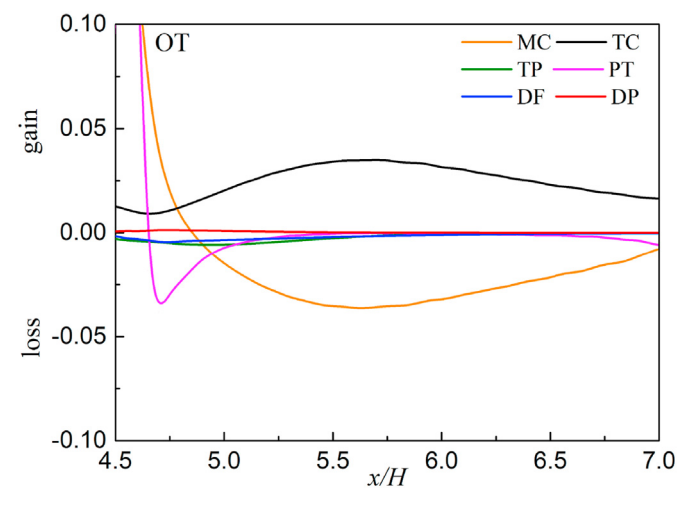


Fig. 9. The MKE budgets of OT showing the standard MKE gain and loss in the OT case.

recovery differently. The research of Yang et al. [20] concluded that the far wake recovery rate is independent of the upwind turbulence structure of the turbine. It has been also proved in Blackman et al. [51] that the TKE budget is influenced by the buildings in the building rear parts and close to the roofs and walls ($\Delta x \leq 1.25H$ and $\Delta z < 1.3H$); and the far wake region within the interested integral domain Ω is insignificantly impacted. Consequently, the tall tree canopy plays a major role in the far wake region to accelerate the wake recovery rates, through transporting MKE to TKE and increasing turbulence production as the TP term shows (e.g. case W1T2). Meanwhile, the low tree canopy (e.g. case W1T1) mainly modifies the strong turbulence production near the shear layer over the street canyon with lower TP term and turbulence intensity. The implications of these physical processes for the stability and performance of the RWT will be further analyzed in Sec. 3.5.

Similarly, the MKE budgets for the higher rooftop turbines W2 and W3 are provided in Fig. A3 of Appendix. The MKE budgets in the turbine wake for W3T2 are less influenced by the buildings and trees due to hub heights being taller than the tree canopy height. The TC, DF and DP terms in W2T2 are slightly affected, demonstrating that the strong shear layer generated by buildings and trees is limited to z/H < 2.

3.4. The wake topology of rooftop wind turbines

The MKE budgets and the spatial distributions in the wake region have been discussed in Sec. 3.3. This section further analyzes the turbine wake propagation impacted by the buildings and trees. Thus, the topology, width and length of the turbine wakes are quantified to answer the second research question in the Introduction. Fig. 12 depicts a qualitative view of the wake topology, which is defined by the iso-surface of streamwise velocity $u_{iso} =$ $0.8u_{hub}$. The wake topology of OT shows disjoint iso-surface behind each turbine aligned in a row without interference. The wake topology of W1 is strongly affected by the buildings and the turbine wakes merge with mean flows over the urban canopy, forming a connected iso-surface. Increasing height of the tree canopy (from W1T1 to W1T3) makes the turbine wakes less distinct in the vertical direction. Moreover, these cases with trees lead to a faster turbine wake recovery than case OT, since the increased turbulence and shear strength (discussed in Fig. 5) contribute to the recovery rate [17]. It is also agreement with the findings in Ref. [52] that the higher incoming turbulence can enhance the mixing process, which result in faster wake recovery. As expected, characteristics of the wakes in W3 converge to case OT, because influence of the building canopy at the hub height z/H = 2 is insignificant. Next, the width and length of the turbine wakes will be quantified.

The standard turbine wake, defined by the velocity deficit, can be described as a Gaussian distribution considering mass and momentum conservation [52–54]. The standard turbine wake is expressed in Eq. (17):

$$\frac{\Delta U}{U_{in}} = \left(1 - \sqrt{1 - \frac{C_T}{8(k^* x/D + \varepsilon)^2}}\right) \exp\left(\frac{1}{2(k^* x/D + \varepsilon)^2} \left\{ \left(\frac{z - z_h}{D}\right)^2 + \left(\frac{y}{D}\right)^2 \right\} \right)$$
(17)

where ΔU is the velocity deficit; U_{in} is the inflow velocity, here we use the spatially averaged (yz-plane) velocity at x/H=4 as the inflow velocity with particular focus on the velocity deficits caused by RWT and trees; x is the streamwise distance referring to wake length; z is the vertical distance; y is the spanwise distance denoting to wake width; z_h is the hub height; $\varepsilon=0.2\sqrt{\beta}$, and $\beta=0.2\sqrt{\beta}$.

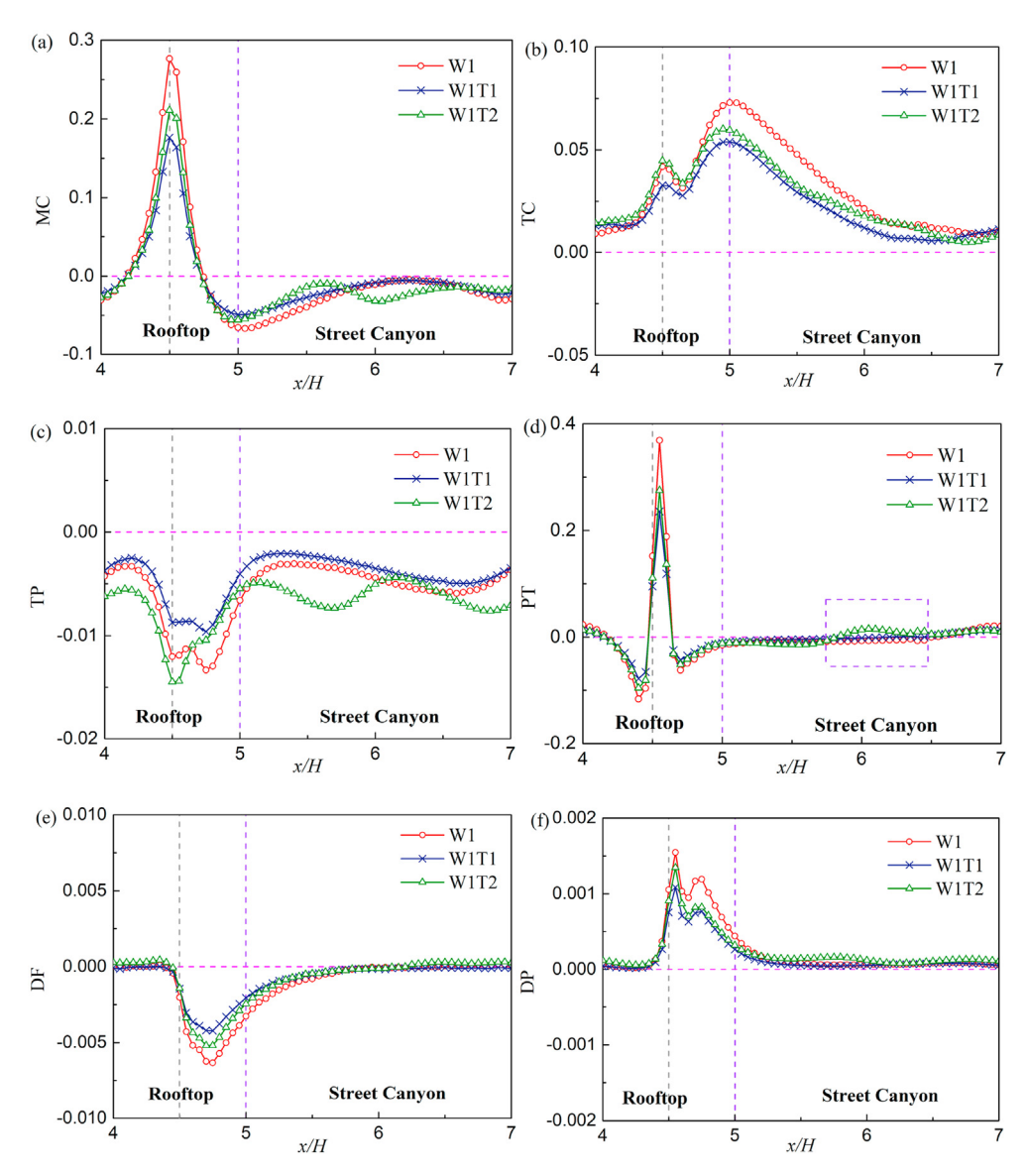


Fig. 10. The MKE budget components of (a) mean convection MC, (b) turbulent transport TC, (c) turbulence production TP, (d) pressure correlation term PT, (e) diffusion DF, and (f) dissipation DP for the lowest turbine W1 with different trees W1T1 and W1T2, where the gray dotted line refers to the location of rooftop turbine and purple dotted line represents the boundary of building and street canyon.

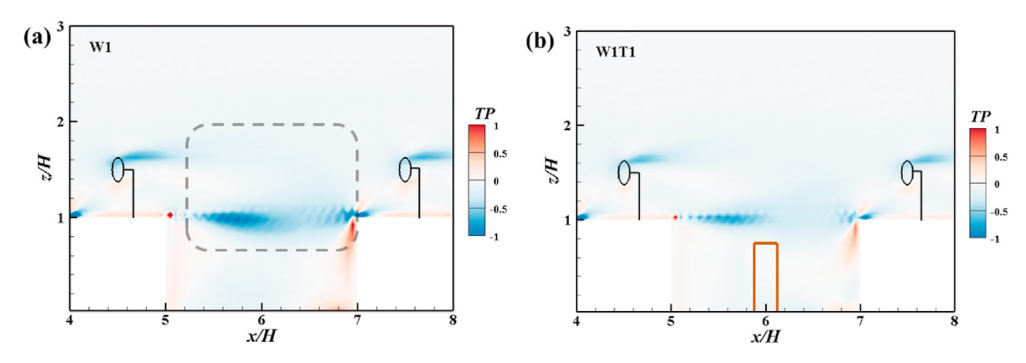


Fig. 11. The contours of *TP* term for the cases of (a) W1 and (b) W1T1 to show the modified budgets by low tree within the street canyon, where the blue (negative component) represents the loss of MKE.

 $\frac{(1+\sqrt{1-C_T})}{2\sqrt{1-C_T}}$; $k^*=\partial\sigma/\partial x$ is the growth rate, σ is the standard deviation of the Gaussian-like velocity deficit profiles at each x. According to the standard deviation and tolerance intervals, about 68% of values

draw in $\pm \sigma$, 95% of values are within $\pm 2\sigma$, and 99.7% are falling in $\pm 3\sigma$ [55].

As shown in Fig. 13, the velocity deficits of RWT are asymmetric and semi-Gaussian under the influence of buildings and tree



Fig. 12. The various wake topologies of the turbine wake in the urban area indicated by iso-surface of streamwise velocity. W1 shows typical wake topologies affected by building canopies; W1T1, W1T2 and W1T3 show the typical turbine wakes influenced by the building and tree canopies, W3 shows the less effected turbine wakes, and OT is the wake only generated by turbines.

canopies (hereinafter, r_w is the wake width, and r is the radius of the turbine disc). The tree canopies can enlarge the velocity deficits below the down tip as the streamwise distance increases (as shown in Fig. 13 (b)). However, when focusing on the shaded region around the turbine disc, it is Gaussian-like and the similar quasiliner assumption in Refs. [16,52] can be applied to calculate the growth rate k^* for obtaining the standard wake of the RWT. The normalized standard deviation of the velocity deficit profile of W1 along the streamwise direction is shown in Appendix (Fig. A4), where $k^* = 0.06$ over the urban canopy is obtained. Compared to results in Refs. [16,52] (case2 to case 5), it is found that the growth rate k^* increases with increasing turbulence intensity. The turbulence intensity in Fig. 4 (b) shows that $I_u = 0.255 - 0.213$ at the hub height z/H = 1.5 - 2, which is higher than that in Refs. [16,52], resulting in larger value of k^* in the current research.

The normalized velocity deficits in spanwise direction for all the cases (except for W1T3, where the tree canopy is at the same height with the turbine hub z/H = 1.5 so that the non-existent semi-Gaussian like velocity deficit is not shown) compared with the standard wake at downward area $\Delta x = 1.0D$ (near wake region) are presented in Fig. 14. The velocity deficits around the turbine disc for all the cases are similar, indicating the turbine wake in spanwise direction and near wake region is slightly affected by tree canopies. The buildings by exerting strong shear forces in vertical direction (see Fig. 5) to promote the recovery of velocity in areas exceeding the up tip and down tip, resulting in the larger wake width. The same criterion of $\pm 2.58\sigma$ in Ref. [55] where 99% of the values falling in this region is adopted to obtained the wake boundary. Compared with the standard wake width of OT $(r_w/r \in [-1.6, 1.6])$, the turbine wake width for the lowest RWT is increased to $r_w/r \in$ [-2.4, 2.4] (about 50%) due to the presence of buildings and tree canopies (Fig. 14 (a)). The identical wake width of RWT with higher hub height (z/H > 1.75 in Fig. 14 (b)) is less affected by the presence of tree canopies, which is consistent with the MKE budgets analysis.

The turbine wake length is evaluated by the normalized velocity deficit at the turbine hub along the streamwise direction as presented in Fig. 15. The MKE budgets (Fig. 10) elucidate that the magnitudes of turbulence production term *TP* and pressure term *PT* in the turbine wake region are increased by the tree canopy.

Therefore, compared to the results in case OT in Fig. 15 (a), the recovery of turbine wakes is accelerated by buildings and trees. For example, the velocity deficit of W1T3 recovers at x/H = 5.5, but that of OT is x/H = 7. The taller tree canopy, smaller tree crown size and closer location to the leeward, the faster recovery rate of the turbine wake. Comparing the results in Figs. 14 and 15, the tree canopy mainly impacts the turbine wake in streamwise direction. As expected, the wake length of the RWT with higher hub height (z/H > 1.75 in Fig. 15 (b)) is less affected.

3.5. Output power of the rooftop wind turbines

The impacts on the power generation of RWT are evaluated in this section. Here, we use two kinds of parameters, output power and normalized power fluctuation, to evaluate the performance of RWT affected by the building and tree canopies. The theoretical time-dependent power output, P(t), of the RWT is calculated based on disc-averaged velocity, which is defined as [56,57]:

$$P(t) = \frac{1}{n} \sum_{i=n} P_i(t) = \frac{1}{n} \sum_{i=n} \frac{1}{2} C_p' \rho \langle V_d \rangle^3 \pi \left(\frac{D}{2}\right)^2$$
 (19)

where n is the number of turbines, $P_i(t)$ is power of the ith turbine, $C_p{'}$ is the local power coefficient, $C_p{'} = \frac{C_p}{(1-\alpha)^3} = \frac{4\alpha}{1-\alpha}$, ρ is the density of air, $\langle V_d \rangle$ is the spatially average velocity of the turbine disc at each second, D is the diameter of the turbine disc. Obviously, the output power depends on the velocity and flow area, which is determined by the fixed geometry of the area swept by the blades. In addition, to evaluate the stability of the RWT, we defined the normalized power fluctuation δ :

$$\delta = \frac{1}{n} \sum_{i=n} \delta_i = \frac{1}{n} \sum_{i=n} \left(\frac{\sigma(P_i(t))}{\overline{P_i(t)}} \right)$$
 (20)

where δ_i is the ratio between the standard deviation of the power and the mean power of the ith turbine, and σ denotes standard deviation.

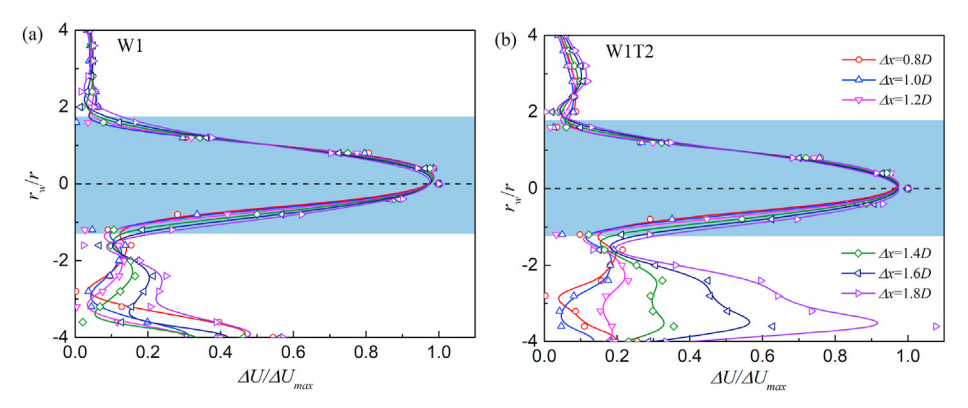


Fig. 13. Vertical distribution of the normalized velocity deficits within the turbine wake for all the cases at downward area of rooftop wind turbine.

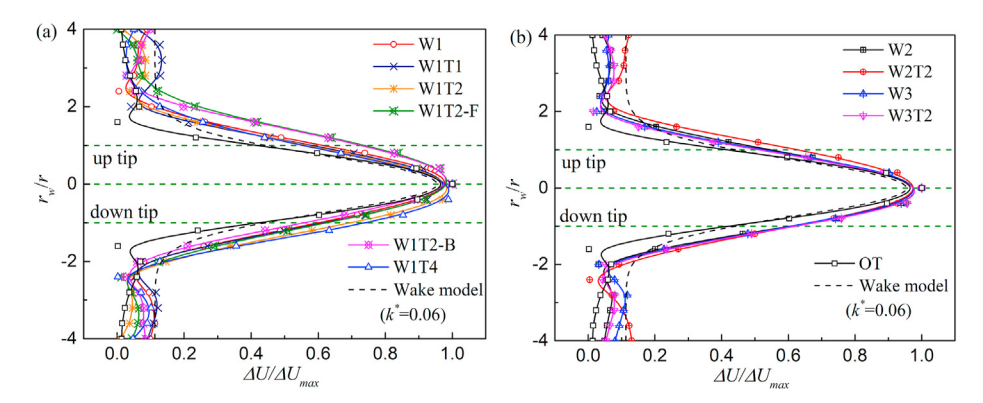


Fig. 14. Spanwise distribution of the normalized velocity deficits in turbine wake for all the cases compared with the standard BP wake model at downward area of turbine with $\Delta x = 1.0D$

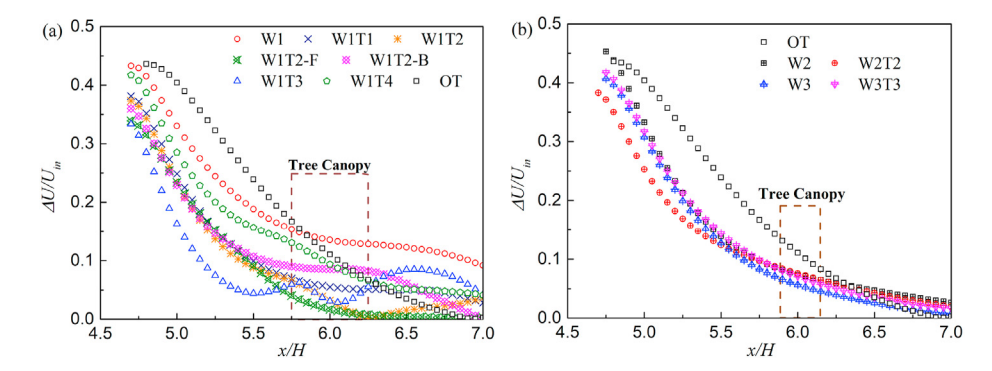


Fig. 15. The normalized velocity deficit at turbine hub versus normalized downwind distance in the wake of turbines: (a) the cases for the lowest turbine W1 with different tree canopies, and (b) the cases for the higher turbines, W2 and W3, with the same tree canopy.

The time-averaged values of P(t) and δ of the RWT are presented in Fig. 16. The averaged power in W1 is 2.26 KW, which agrees well with the power obtained experimentally and numerically for small rooftop turbines [12,58,59]. The tall tree (W1T2, W1T3) has a distinct negative effect on the performance of turbines, resulting in decreased power outputs and increased power fluctuations. This is related to the fact that the tall trees extract mean momentum (see Fig. 8) and transform more MKE to TKE with increased turbulence production (see Fig. 10). Instead, the low tree canopy (W1T1) is beneficial for improving the performance of the RWT, which can improve the power output by 4.9% and decrease δ by 2.8% with respect to the case W1. Although the low tree canopy has little effect on the mean momentum (see Figs. 7 (c) and Fig. 8 (c)), it modulates the turbulence production (see Fig. 11) near the strong shear-layer at the roof level and decreases TKE and turbulence intensity (see Fig. 6 (c)) within the street canyon.

To further validate the potential benefits of the low tree canopy, we conducted the other three cases with different tree morphologies W1T1-L, W1T1-S and W1T1-W. Here, W1T1-L means that the location of maximum leaf area density of T1 is low as $z_m/h = 0.5$, W1T1-S refers to that the leaf area density of T1 is sparse as $a_m = 0.5$, and W1T1-W denotes that the crown size of T1 is wide as Rt/H = 0.5. As shown in the Fig. A5 and Fig. A6 of Appendix, the wider and denser tree canopies improve the performance of RWT, in which the power is increased by 16.6% and the normalized power fluctuation is reduced by 5.2% in W1T1-W compared to W1. Based on these results, it can be posited that tall tree canopy negatively impacts the mean power output and power fluctuation of RWT; in contrast, the low tree canopy with dense foliage and wide crown size can reduce the power fluctuations, which is a desirable effect.

4. Conclusions

The joint aerodynamic impact of buildings and street trees on the wake propagation and performance of rooftop wind turbines are investigated using an open-source large-eddy simulation model. Several cases of different tree morphologies and turbine hub heights in urban street canyon with moderate aspect ratio (H/W=0.5) are conducted. The spatial distribution of flow field, MKE budgets and the wake topology of RWT are discussed. The key

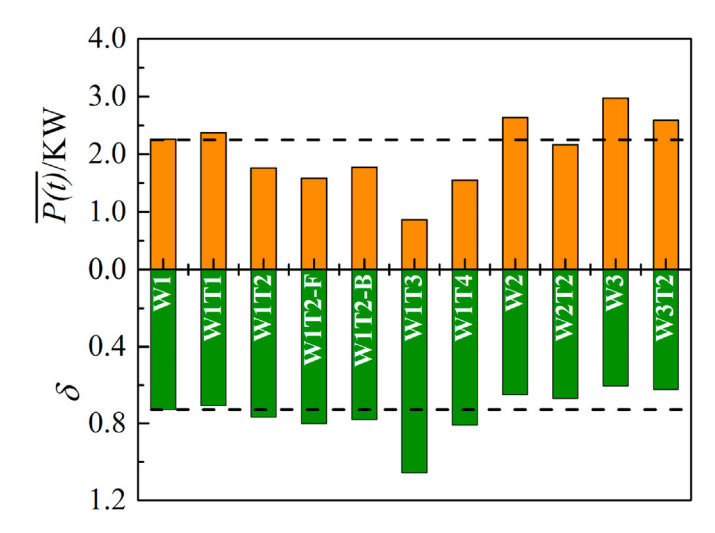


Fig. 16. The averaged output powers and normalized power fluctuations of the RWT for all the cases, where the dotted lines indicate the baseline based on W1.

findings in addressing two research questions raised in Section 1 are summarized below:

- 1) Tree canopy taller than the mean building height modifies the existing strong shear layer above the building canopy by inducing a significant increase in the momentum flux and turbulence production, producing the most drastic change to the streamwise velocity field and negative effects on the performance of the rooftop turbines within a limited distance from the hub-height for z/H < 2.
- 2) Tree canopies lower than the buildings seldom alter the mean flow and canyon circulation patterns, but they significantly reduce the turbulence production and lower the turbulence intensity, causing positive effects on the performance of the rooftop turbines by having a lower power fluctuation and higher mean power output. This benefit is more distinct for the trees with denser foliage, wider crown size and higher location of maximum leaf area density.
- 3) The asymmetric wake topology of the low turbines shows downward tendencies due to the drag of building and tree canopies, accompanied with an enlarged wake width $r_w/r \in [-2.4.2.4]$.
- 4) The recovery rate of the turbine wake in the streamwise direction is significantly improved by the strong pressure gradients of the tree canopies through magnifying the turbulence production *TP* and pressure term *PT* in the far wake region, resulting in a shortened wake length.

Overall, this study is limited by the idealized tree morphology as

well as the assumption of an 'infinite' rooftop wind turbine arrays. Nevertheless, the results reveal nontrivial impacts of street trees on urban environmental flows and subsequent influences on the turbine performance. Our first attempt of quantifying the impacts of complex urban environmental flows can inform assessment of wind energy resources in the built environment depending on seasonality, especially conditions of leaves-on versus no-leaves. It is expected that future research based on field and laboratory measurements will provide additional insights into the practical significance of vegetation on the design and performance rooftop wind turbines.

CRediT authorship contribution statement

Xiantao Fan: Methodology, Investigation, Formal analysis, Writing — original draft. **Mingwei Ge:** Resources, Writing — review & editing. **Wei Tan:** Validation. **Qi Li:** Conceptualization, Resources, Supervision, Writing — review & editing.

Declaration of competing interest

The authors declare that they have no known competing financial interests or personal relationships that could have appeared to influence the work reported in this paper.

Appendix

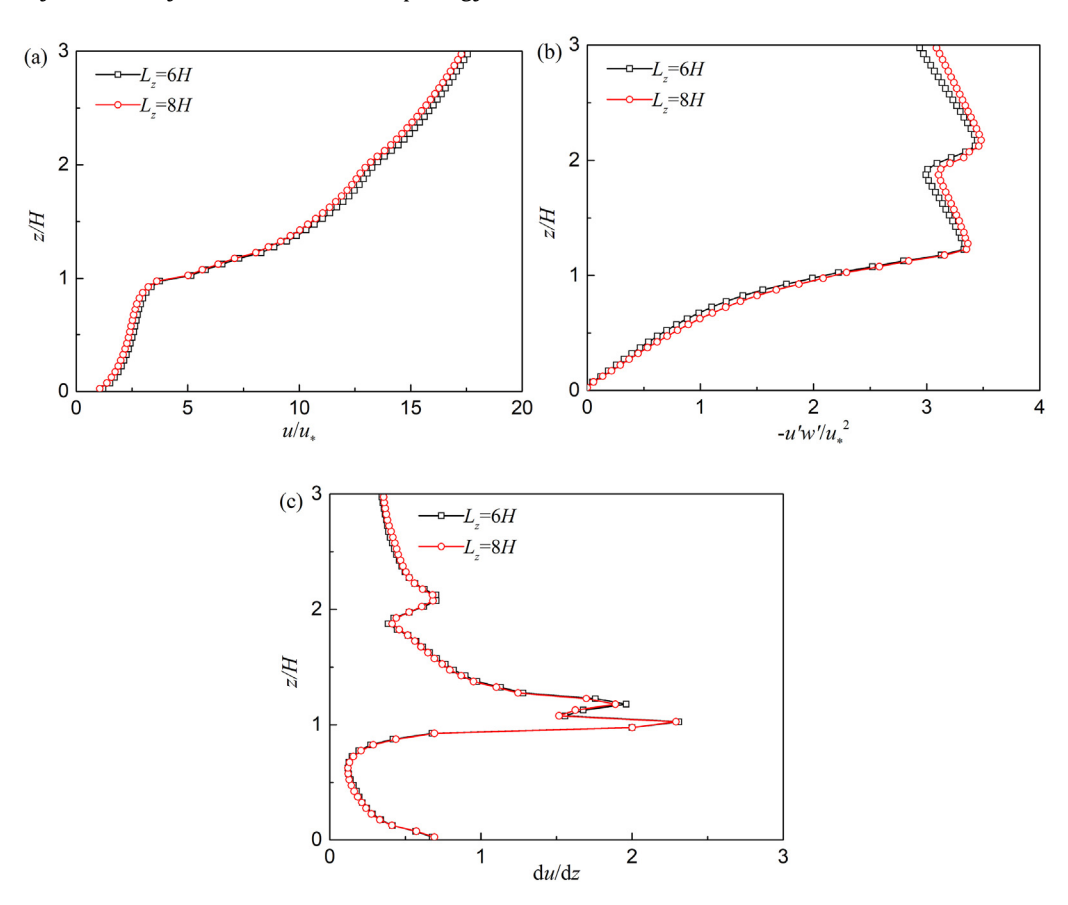


Fig. A1. The verification of the vertical domain size Lz (a) the mean velocity, (b) the mean Reynolds stress and (c) the streamwise velocity gradient

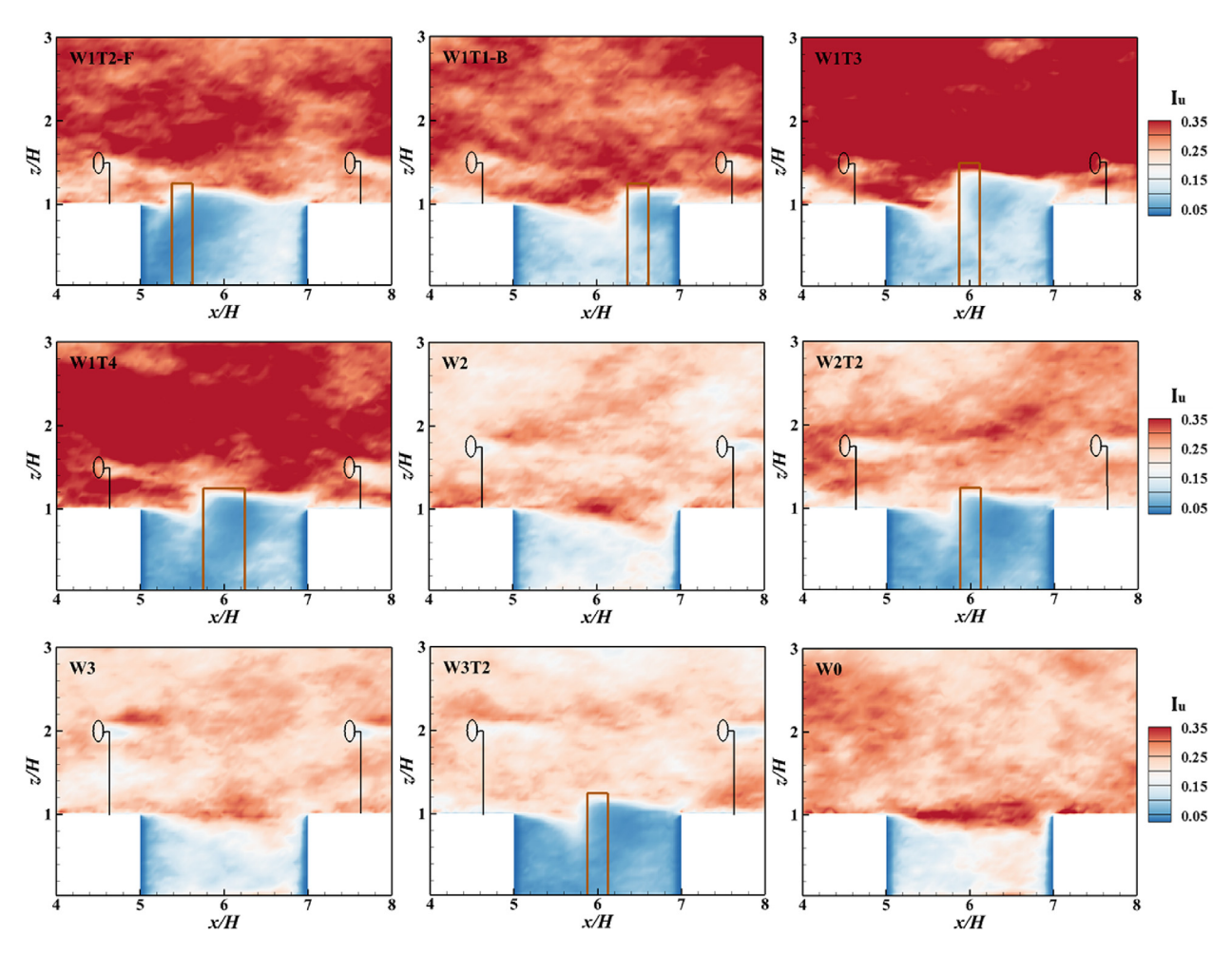


Fig. A2. The turbulence intensity in the middle xz-plane for all the cases except W1, W1T1 and W1T2

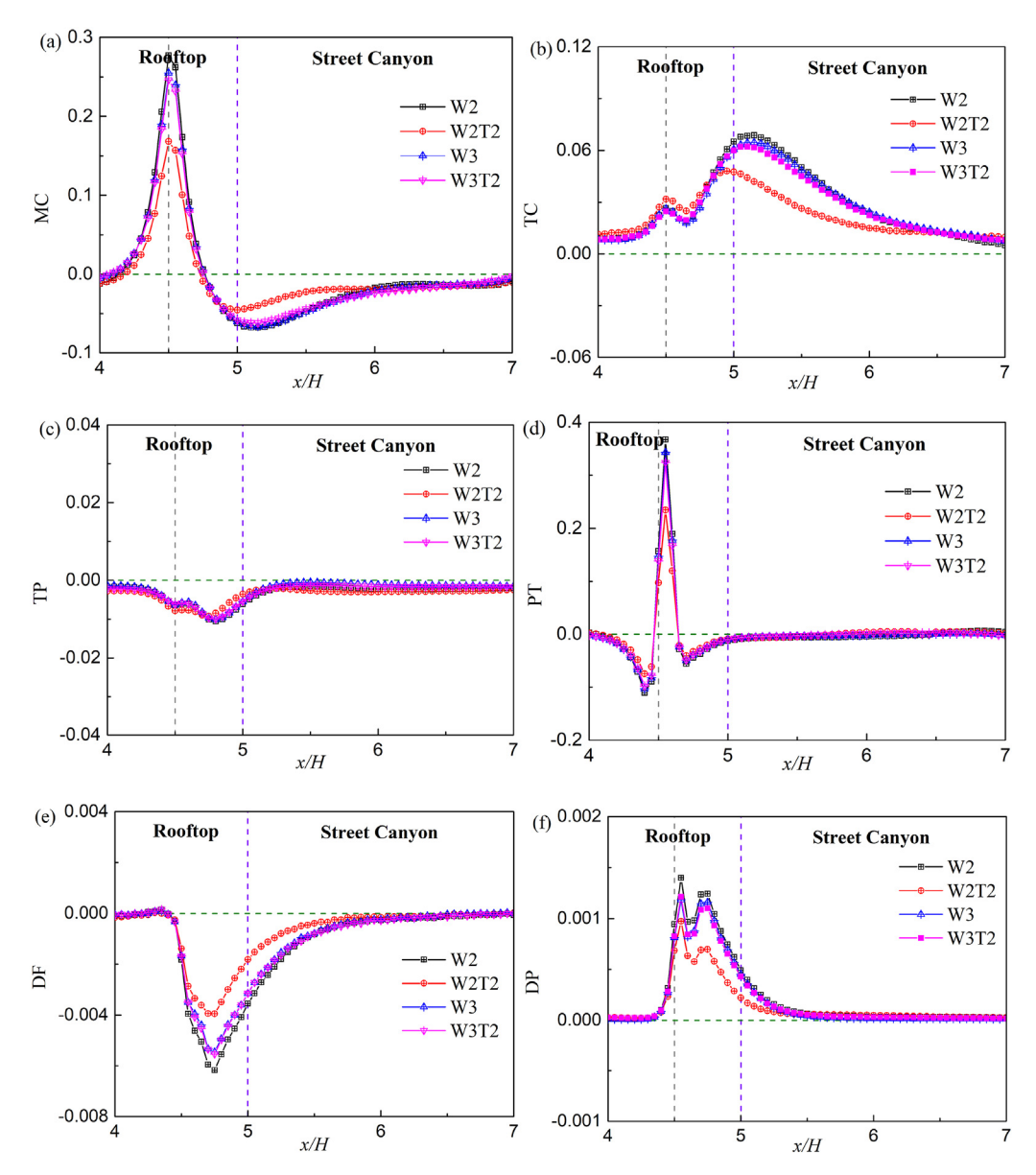
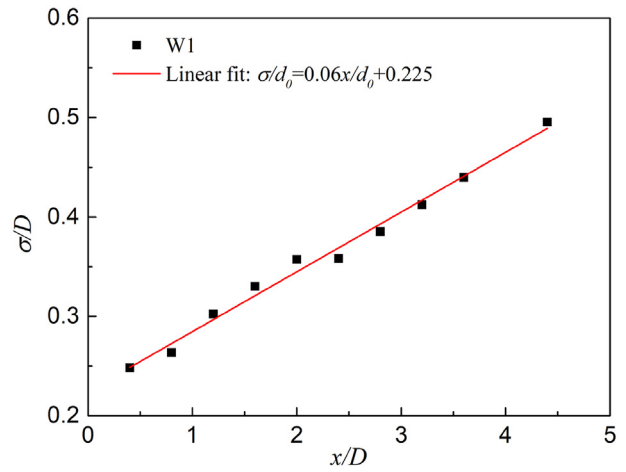


Fig. A3. The MKE budget components of (a) mean convection MC, (b) turbulent transport TC, (c) turbulence production TP, (d) pressure correlation term PT, (e) diffusion DF, and (f) dissipation DP for the two higher turbines, W2 and W3, with the same tree canopy, where the gray dotted line refers to the location of rooftop turbine



 $\textbf{Fig. A4.} \ \ \text{The normalized standard deviation of the Gaussian-like velocity deficit profile} \\ \ \ \text{of W1}$

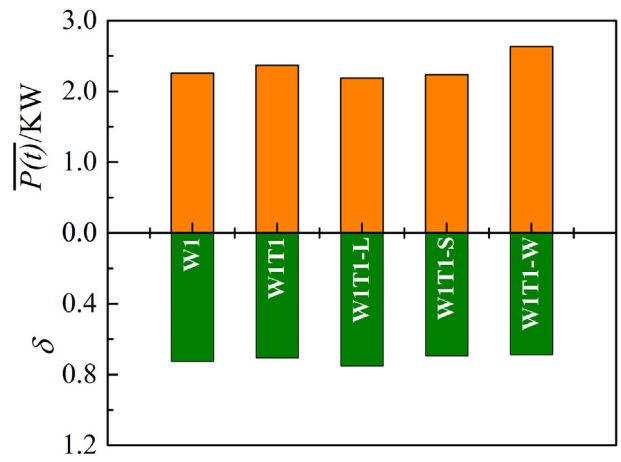


Fig. A5. The averaged output powers and power fluctuation of the RWT for W1T1-L (the location of maximum leaf area density of T1 is low as $z_m/h = 0.5$), W1T1-S (the leaf area density of T1 is small as $a_m = 0.5$), and W1T1-W (the crown size of T1 is wide as Rt/H = 0.5)

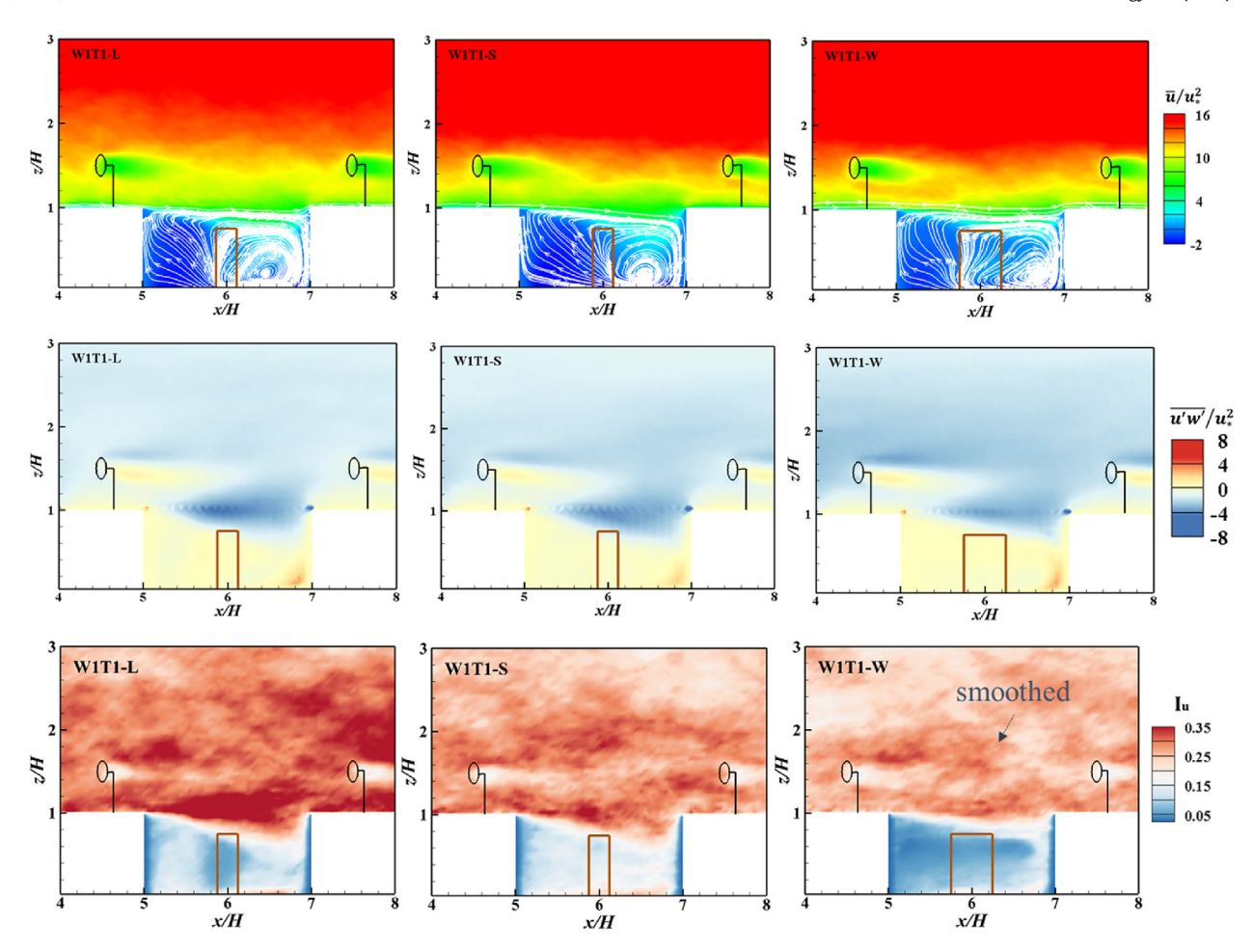


Fig. A6. The normalized time-average velocity contours (top), moment flux (middle) and turbulence intensity (bottom) in the middle xz-plane for W1T1-L, W1T1-S, and W1T1-W

References

- [1] A. Kc, J. Whale, T. Urmee, Urban wind conditions and small wind turbines in the built environment: a review, Renew. Energy 131 (2019) 268–283.
- [2] Z. Tasneem, A. Al Noman, S.K. Das, D.K. Saha, M.R. Islam, M.F. Ali, et al., An analytical review on the evaluation of wind resource and wind turbine for urban application: prospect and challenges, Dev.Built. Environ. 4 (2020).
- [3] D. Ayhan, Ş. Sağlam, A technical review of building-mounted wind power systems and a sample simulation model, Renew. Sustain. Energy Rev. 16 (1) (2012) 1040–1049.
- [4] A. Rezaeiha, H. Montazeri, B. Blocken, A framework for preliminary large-scale urban wind energy potential assessment: roof-mounted wind turbines, Energy Convers. Manag. 214 (2020) 112770.
- [5] M. Ghasemian, Z.N. Ashrafi, A. Sedaghat, A review on computational fluid dynamic simulation techniques for Darrieus vertical axis wind turbines, Energy Convers. Manag. 149 (2017) 87–100.
- [6] Y. Tripanagnostopoulos, A. Christodoulou, S. Tselepis, M. Souliotis, J. Tonui, Practical aspects for small wind turbine applications, Proc Int EWEC 7 (2004).
- [7] S. Li, Y. Li, C. Yang, Q. Wang, B. Zhao, D. Li, et al., Experimental investigation of solidity and other characteristics on dual vertical axis wind turbines in an urban environment, Energy Convers. Manag. (2021) 229.
- [8] F. Toja-Silva, O. Lopez-Garcia, C. Peralta, J. Navarro, I. Cruz, An empirical—heuristic optimization of the building-roof geometry for urban wind energy exploitation on high-rise buildings, Appl. Energy 164 (2016) 769–794.
- [9] A.B. Tabrizi, J. Whale, T. Lyons, T. Urmee, Performance and safety of rooftop wind turbines: use of CFD to gain insight into inflow conditions, Renew. Energy 67 (2014) 242–251.
- [10] I. Abohela, N. Hamza, S. Dudek, Effect of roof shape, wind direction, building height and urban configuration on the energy yield and positioning of roof mounted wind turbines, Renew. Energy 50 (2013) 1106–1118.
- [11] H.Y. Peng, S.F. Dai, K. Lin, G. Hu, H.J. Liu, Experimental investigation of wind characteristics and wind energy potential over rooftops: effects of building parameters, J. Wind Eng. Ind. Aerod. 205 (2020) 104304.
- [12] F. Balduzzi, A. Bianchini, E.A. Carnevale, L. Ferrari, S. Magnani, Feasibility analysis of a Darrieus vertical-axis wind turbine installation in the rooftop of a building, Appl. Energy 97 (2012) 921–929.

- [13] R.J. Barthelmie, K. Hansen, S.T. Frandsen, O. Rathmann, J.G. Schepers, W. Schlez, et al., Modelling and measuring flow and wind turbine wakes in large wind farms offshore, Wind Energy 12 (5) (2009) 431–444.
- [14] L.J. Vermeer, J.N. Sørensen, A. Crespo, Wind turbine wake aerodynamics, Prog. Aero. Sci. 39 (6–7) (2003) 467–510.
- [15] F. Porté-Agel, Y.-T. Wu, C.-H. Chen, A numerical study of the effects of wind direction on turbine wakes and power losses in a large wind farm, Energies 6 (10) (2013) 5297–5313.
- [16] M. Abkar, F. Porté-Agel, Influence of atmospheric stability on wind-turbine wakes: a large-eddy simulation study, Phys. Fluids 27 (3) (2015), 035104.
- [17] Y.-T. Wu, F. Porté-Agel, Atmospheric turbulence effects on wind-turbine wakes: an LES study, Energies 5 (12) (2012) 5340–5362.
- [18] B. Du, M. Ge, C. Zeng, G. Cui, Y. Liu, Influence of atmospheric stability on wind-turbine wakes with a certain hub-height turbulence intensity, Phys. Fluids 33 (5) (2021).
- [19] M. Ge, S. Zhang, H. Meng, H. Ma, Study on interaction between the wind-turbine wake and the urban district model by large eddy simulation, Renew. Energy 157 (2020) 941–950.
- [20] X. Yang, K.B. Howard, M. Guala, F. Sotiropoulos, Effects of a three-dimensional hill on the wake characteristics of a model wind turbine, Phys. Fluids 27 (2) (2015), 025103.
- [21] M. Ge, D.F. Gayme, C. Meneveau, Large-eddy simulation of wind turbines immersed in the wake of a cube-shaped building, Renew. Energy 163 (2021) 1063–1077.
- [22] S.E. Belcher, I.N. Harman, J.J. Finnigan, The wind in the willows: flows in forest canopies in complex terrain, Annu. Rev. Fluid Mech. 44 (1) (2012) 479–504.
- [23] M.G. Giometto, A. Christen, P.E. Egli, M.F. Schmid, R.T. Tooke, N.C. Coops, et al., Effects of trees on mean wind, turbulence and momentum exchange within and above a real urban environment, Adv. Water Resour. 106 (2017) 154–168.
- [24] C. Wang, Q. Li, Z.-H. Wang, Quantifying the impact of urban trees on passive pollutant dispersion using a coupled large-eddy simulation—Lagrangian stochastic model, Build. Environ. 145 (2018) 33—49.
- [25] Y. Pan, M. Chamecki, S.A. Isard, Large-eddy simulation of turbulence and particle dispersion inside the canopy roughness sublayer, J. Fluid Mech. 753 (2014) 499–534.
- [26] Q. Li, Z.-H. Wang, Large-eddy simulation of the impact of urban trees on

- momentum and heat fluxes, Agric. For. Meteorol. 255 (2018) 44-56.
- [27] E.S. Krayenhoff, J.L. Santiago, A. Martilli, A. Christen, T.R. Oke, Parametrization of drag and turbulence for urban neighbourhoods with trees, Boundary-Layer Meteorol. 156 (2) (2015) 157–189.
- [28] C. Gromke, B. Ruck, Aerodynamic modelling of trees for small-scale wind tunnel studies, Forestry 81 (3) (2008) 243–258.
- [29] A. Jimenez, A. Crespo, E. Migoya, J. Garcia, Advances in large-eddy simulation of a wind turbine wake, J. Phys. Conf. 75 (2007), 012041.
- [30] Y.H. Tseng, C. Meneveau, M.B. Parlange, Modeling flow around bluff bodies and predicting urban dispersion using large eddy simulation, Environ. Sci. Technol. 40 (8) (2006) 2653–2662.
- [31] S. Chester, C. Meneveau, M.B. Parlange, Modeling turbulent flow over fractal trees with renormalized numerical simulation, J. Comput. Phys. 225 (1) (2007) 427–448.
- [32] Q. Li, E. Bou-Zeid, W. Anderson, The impact and treatment of the Gibbs phenomenon in immersed boundary method simulations of momentum and scalar transport, J. Comput. Phys. 310 (2016) 237–251.
- [33] M. Calaf, C. Meneveau, J. Meyers, Large eddy simulation study of fully developed wind-turbine array boundary layers, Phys. Fluids 22 (1) (2010), 015110
- [34] C. Shapiro, D. Gayme, C. Meneveau, Filtered actuator disks: theory and application to wind turbine models in large eddy simulation, Wind Energy 22 (2019).
- [35] Q. Li, E. Bou-Zeid, W. Anderson, S. Grimmond, M. Hultmark, Quality and reliability of LES of convective scalar transfer at high Reynolds numbers, Int. J. Heat Mass Tran. 102 (2016) 959–970.
- [36] E. Bou-Zeid, C. Meneveau, M. Parlange, A scale-dependent Lagrangian dynamic model for large eddy simulation of complex turbulent flows, Phys. Fluids 17 (2) (2005), 025105.
- [37] H. Zhang, M. Ge, Y. Liu, X.I.A. Yang, A new coupled model for the equivalent roughness heights of wind farms, Renew. Energy 171 (2021) 34–46.
- [38] M. Ge, H. Yang, H. Zhang, Y. Zuo, A prediction model for vertical turbulence momentum flux above infinite wind farms, Phys. Fluids 33 (5) (2021).
- [39] F. Porté-Agel, Y.-T. Wu, H. Lu, R.J. Conzemius, Large-eddy simulation of atmospheric boundary layer flow through wind turbines and wind farms, J. Wind Eng. Ind. Aerod. 99 (4) (2011) 154–168.
- [40] A. Niayifar, F. Porté-Agel, A new analytical model for wind farm power prediction, J. Phys. Conf. 625 (2015), 012039.
- [41] B. Lalic, D.T. Mihailovic, An empirical relation describing leaf-area density inside the forest for environmental modeling, J. Appl. Meteorol. 43 (4) (2004) 641–645.
- [42] X.I.A. Yang, J. Sadique, R. Mittal, C. Meneveau, Integral wall model for large eddy simulations of wall-bounded turbulent flows, Phys. Fluids 27 (2) (2015), 025112.
- [43] X.I.A. Yang, H.H.A. Xu, X.L.D. Huang, M.W. Ge, Drag forces on sparsely packed

- cube arrays, J. Fluid Mech. 880 (2019) 992-1019.
- [44] D. Poggi, A. Porporato, L. Ridolfi, J.D. Albertson, G.G. Katul, Interaction between large and small scales in the canopy sublayer, Geophys. Res. Lett. 31 (5) (2004) n/a-n/a.
- [45] C.-H. Liu, M.C. Barth, D.Y.C. Leung, Large-eddy simulation of flow and pollutant transport in street canyons of different building-height-to-street-width ratios, J. Appl. Meteorol. 43 (10) (2004) 1410–1424.
- [46] L. Soulhac, R.J. Perkins, P. Salizzoni, Flow in a street canyon for any external wind direction, Boundary-Layer Meteorol. 126 (3) (2007) 365–388.
- [47] G.M. Martínez, F. Valero, L. Vázquez, The TKE budget in the convective Martian planetary boundary layer, Q. J. R. Meteorol. Soc. 137 (661) (2011) 2194–2208.
- [48] W. Yue, C. Meneveau, M.B. Parlange, W. Zhu, H.S. Kang, J. Katz, Turbulent kinetic energy budgets in a model canopy: comparisons between LES and wind-tunnel experiments, Environ. Fluid Mech. 8 (1) (2008) 73–95.
- [49] X. Liu, F.O. Thomas, Measurement of the turbulent kinetic energy budget of a planar wake flow in pressure gradients, Exp. Fluid 37 (4) (2004) 469–482.
- [50] M.J. Dwyer, E.G. Patton, R.H. Shaw, Turbulent kinetic energy budgets from a large-eddy simulation of airflow above and within a forest canopy, Boundary-Layer Meteorol. 84 (1) (1997) 23–43.
- [51] K. Blackman, L. Perret, I. Calmet, C. Rivet, Turbulent kinetic energy budget in the boundary layer developing over an urban-like rough wall using PIV, Phys. Fluids 29 (8) (2017), 085113.
- [52] M. Bastankhah, F. Porté-Agel, A new analytical model for wind-turbine wakes, Renew. Energy 70 (2014) 116–123.
 [53] M. Ge, Y. Wu, Y. Liu, Q. Li, A two-dimensional model based on the expansion of
- [53] M. Ge, Y. Wu, Y. Liu, Q. Li, A two-dimensional model based on the expansion of physical wake boundary for wind-turbine wakes, Appl. Energy 233—234 (2019) 975—984.
- [54] M. Ge, Y. Wu, Y. Liu, X.I.A. Yang, A two-dimensional Jensen model with a Gaussian-shaped velocity deficit, Renew. Energy 141 (2019) 46–56.
- [55] X. Gao, H. Yang, L. Lu, Optimization of wind turbine layout position in a wind farm using a newly-developed two-dimensional wake model, Appl. Energy 174 (2016) 192–200.
- [56] X. Fan, Z. Wang, X. Chen, Y. Wang, W. Tan, Experimental investigation on flow-induced vibration of flexible multi cylinders in atmospheric boundary layer, Int. J. Mech. Sci. (2020) 105815.
- [57] M. Huleihil, G. Mazor, Wind turbine power: the betz limit and beyond, Advances in Wind Power (2012) 3–29.
- [58] S. Zanforlin, S. Letizia, Effects of upstream buildings on the performance of a synergistic roof-and-diffuser augmentation system for cross flow wind turbines, J. Wind Eng. Ind. Aerod. 184 (2019) 329–341.
- [59] K.-Y. Lee, S.-H. Tsao, C.-W. Tzeng, H.-J. Lin, Influence of the vertical wind and wind direction on the power output of a small vertical-axis wind turbine installed on the rooftop of a building, Appl. Energy 209 (2018) 383–391.